Environmental Research 265 (2025) 120393

Contents lists available at ScienceDirect

Environmental Research

journal homepage: www.elsevier.com/locate/envres

# A comprehensive library of lifetime physiological equations for PBK models: Enhancing dietary exposure modeling with mercury as a case study

Thomas Gastellu [a,b], Achilleas Karakoltzidis [c,d], Aude Ratier [e,f], Marie Bellouard [g,h], Jean-Claude Alvarez [g,h], Bruno Le Bizec [a], Gilles Rivière [b], Spyros Karakitsios [c,d], Dimosthenis A. Sarigiannis [c,d], Carolina Vogs [i,j,*]

[a] Oniris, INRAE, LABERCA, Nantes, 44300, France
[b] Risk Assessment Department - French Agency for Food, Environmental and Occupational Health and Safety (ANSES), Maisons-Alfort, 94700, France
[c] Aristotle University of Thessaloniki, Department of Chemical Engineering, Environmental Engineering Laboratory, University Campus, Thessaloniki 54124, Greece
[d] HERACLES Research Center on the Exposome and Health, Center for Interdisciplinary Research and Innovation, Balkan Center, Bldg. B, 10th km Thessaloniki – Thermi Road, 57001, Greece
[e] INERIS, Unit of Experimental Toxicology and Modelling, Verneuil-en-Halatte, France
[f] PériTox Laboratory, UMR-I 01 INERIS, Université de Picardie Jules Verne, Amiens, France
[g] Department of Pharmacology and Toxicology, Raymond Poincaré hospital, GHU AP-HP.Paris-Saclay, 92380 Garches, France
[h] Paris-Saclay/Versailles University, Inserm U-1018, CESP, Team MOODS, Garches, France
[i] Department of Animal Biosciences, Swedish University of Agricultural Sciences (SLU), Uppsala, Sweden
[j] Institute of Environmental Medicine, Karolinska Institutet, Stockholm, Sweden

ARTICLE INFO

*Keywords:*
ADME toxicokinetics
Lifetime dietary exposure
total mercury
Toxicological reference values

ABSTRACT

Dietary risk assessment of food contaminants requires a well-established understanding of the exposure in a heterogeneous population. There are many methods for estimating human exposure to food contaminants, such as intake calculations and internal biomarkers of exposure measured in individuals. However, those methods are expensive, partly invasive, and often provide a momentary exposure snapshot. Physiologically Based Kinetic (PBK) modelling is increasingly used to overcome those challenges that traditional human exposure methods encounter. Still, PBK models are often restricted to certain life stages (e.g., children, adolescents, adults). This study outlines a strategy for implementing nonlinear organ growths in age-specific PBK models to enhance dietary risk assessment from lifetime exposure. To this end, lifetime physiological equations calculating organ growth for both sexes were inventoried from literature and a library was established for 24 organs. We then assessed total lifelong mercury exposure via foodstuff by combining two existing age-specific PBK models for methylmercury (MeHg) and inorganic mercury (iHg) that simulated internal exposure to total mercury, the speciation typically measured in hair and urine. We implemented a set of physiological equations in the PBK model that fitted best the total mercury measured in individuals' organs, hair, and urine from heterogeneous populations. For refined dietary risk assessment, we ultimately estimated total mercury concentration in hair and urine based on i) maximum limits defined by the regulation for MeHg in seafood, ii) the health-based guidance values for MeHg and iHg, and iii) realistic intakes considering French demographic parameters and food consumption data. These exposure scenarios demonstrated that total mercury concentrations in hair and urine estimated from realistic intakes are below critical effect level measures at all ages. The result of this study is the creation of easily accessible tools in Excel and R that facilitate the implementation of physiological equations in Next Generation PBK models.

## 1. Introduction

The general population is chronically exposed to various chemicals from foodstuffs throughout its lifetime, thereby increasing the risk of triggering adverse health effects (Doménech and Martorell, 2024; EFSA, 2011). To assess the risk of chemicals in food, the chemical hazard is

* Corresponding author. Department of Animal Biosciences, Swedish University of Agricultural Sciences (SLU), Uppsala. Sweden.
*E-mail address:* Carolina.vogs@slu.se (C. Vogs).

https://doi.org/10.1016/j.envres.2024.120393
Received 29 August 2024; Received in revised form 8 October 2024; Accepted 17 November 2024
Available online 22 November 2024

characterized in conjunction with the exposure levels of the population throughout a lifespan (WHO and IPCS, 2021). Therefore, dietary exposure is commonly estimated by a real-life intake based on the frequency and amount consumed and the chemical concentrations measured in food (ANSES, 2011; Beronius et al., 2020; EFSA, 2021; Gbadamosi et al., 2021; Pruvost-Couvreur et al., 2020a). For food safety assessment, those estimated real-life intakes are then compared to health-based guidance values (HBGV), such as a tolerable daily intake (TDI) or a risk characterization ratio. An HBGV represents a chemical's maximum acceptable intake level to prevent its most critical adverse health effects (Doménech and Martorell, 2024; Pruvost-Couvreur et al., 2020a). However, this risk assessment procedure often overlooks the amount of a chemical that accumulates in different body parts over the course of chronic exposure.

Another method for assessing exposure to contaminants is to determine chemical concentrations in biological matrices (e.g., blood, urine, hair, or breast milk) sampled from individuals. Those exposure measurements are biomarkers of internal exposure and are often collected in human biomonitoring (HBM) studies (Bizjak et al., 2022; Jeddi et al., 2022; Santonen et al., 2023). Internal exposure results from chemical-specific toxicokinetic processes, i.e., the absorbed dose that reaches the circulating blood system and distributes to the organs/tissues of interest, including eliminating organs (McCarty et al., 2011). Toxicokinetic processes in risk assessment are considered by comparing measured internal exposure to available human biomonitoring guidance value (HBM-GV), thereby improving the evaluation of potential health effects in a population (WHO & IPCS, 2021). Although HBM data provide substantial information on internal exposure, their collection can often be considered invasive and costly. In addition, a single sample is typically collected at one time point to monitor internal exposure aggregated from multiple sources and pathways in individuals (Arnold et al., 2013). Consequently, the origin of the chemical exposure is difficult to identify, and the sampling timing may strongly affect the concentrations measured in biological matrices (Dede et al., 2018). Furthermore, it is difficult to comprehensively collect other important co-variates that influence the occurrence of a health effect (e.g., the chemical toxicity in different subpopulations, the sensitivity of the exposed individual and of a subpopulation, the duration and route of exposure (Buist, 2010) as well as the dose magnitude).

Advanced methodologies to determine dietary intake include exposure reconstruction using exposure biomarkers and computational models (Georgopoulos et al., 2009). These approaches support the application of computational New Approach Methodologies (NAMs) in the regulatory field (Deepika & Kumar, 2023). Computational toxicokinetic models were shown to complement human biomonitoring as a non-invasive and non-expensive tool, particularly when reliably calibrated. Indeed, physiologically based kinetic (PBK) models support the prediction of internal exposure in multiple organs, including target, storage, and elimination organs, for all simulated time points and across exposure doses (Zhang et al., 2024). PBK models thereby simulate the toxicokinetic processes of Absorption, Distribution, Metabolism, and Excretion (ADME) within the body by combining numerous compartments (organs) connected by blood flows (WHO and IPCS, 2010). The structure of PBK models enables several exposure routes to be aggregated, including ingestion, inhalation, and dermal exposure. The internal exposure is thereby estimated based on all external sources by simulating an established PBK model forward. Inversely, PBK models estimate the external exposures when considering the biomarker of exposure concentrations by applying reverse dosimetry (Dopart and Friesen, 2017; Georgopoulos et al., 2009; HBM4EU, 2018; Yoon et al., 2022).

In most cases, PBK models are established for a certain life stage, such as childhood, adulthood, or pregnancy. Internal exposures across specific life stages can also be extrapolated (WHO and IPCS, 2021), but this application is challenging due to complex physiological changes. Current practice relies on using physiological parameters that are commonly defined as fractions of body weight and cardiac output to calculate organ volumes and blood flows to the organs, respectively. In contrast, several lifetime PBK models implemented various non-linear physiological equations for different organ growths to model lifetime exposure across life stages (Beaudouin et al., 2010; Deepika et al., 2021; Haddad et al., 2001, 2006; Mallick et al., 2020; Pendse et al., 2020; Price et al., 2003; Ring et al., 2017; Sarigiannis et al., 2020; Smith et al., 2014; Verner et al., 2008; Wu et al., 2015). Considering these nonlinear physiological changes enables a less uncertain estimation of the chemical concentrations in biological matrices for different ages. To facilitate the establishment of lifetime PBK models for any chemical, existing non-linear physiological equations for organ growths, including refinement for adipose tissues, muscles, and the brain (Schlender et al., 2016) need to be documented in a user-friendly and applicable manner.

The present study aimed to establish a strategy for implementing physiological equations in PBK models to enhance the assessment of chemical risk in food from lifetime dietary exposure, illustrated by mercury contamination in food as a case study. To this end, we 1) established a library of physiological equations describing organ volume increases over a lifespan, 2) estimated internal exposure to total mercury by modeling chronic dietary exposure to methylmercury (MeHg) and inorganic mercury (iHg) in a virtual population considering different socio-economic and socio-demographic parameters as well as French food consumption data, and 3) compared total mercury concentrations in hair and urine estimated by three intake scenarios (i.e., real lifetime intakes, maximum MeHg levels in seafood, HBGVs for MeHg and iHg) with HBM-GV. This study produced a user-friendly Excel sheet and an R code for applying the inventory of physiological equations in the Next Generation PBK models needed for refined dietary risk assessment.

## 2. Materials and methods

Fig. 1 illustrates our general workflow, encompassing a literature review on lifetime PBK models, followed by their application in modifying age-specific PBK models for chronic total mercury exposure.

### 2.1. Inventory of lifetime physiological equations

A library of lifetime physiological equations was assembled for 24 organs/tissues that were extracted from lifetime PBK models. Seven lifetime PBK models published before April 2023 (Ratier et al., 2023) were directly identified (Deepika et al., 2021; Mallick et al., 2020; Pendse et al., 2020; Sarigiannis et al., 2020; Smith et al., 2014; Verner et al., 2008; Wu et al., 2015), that further highlighted five additional lifetime PBK models (Beaudouin et al., 2010; Haddad et al., 2001, 2006; Price et al., 2003; Ring et al., 2017). We synthesized a library of lifetime physiological equations based on the 12 reviewed lifetime PBK models. An overview of the reviewed lifetime PBK models is provided in Table 1, including their application of substance family and specific substances, number of compartments, and exposure routes. Table 2 lists the original publications that have been used to parametrize the physiological equations of organ growth as reported in the different lifetime PBK models. The inventory was synthesized in a user-friendly Excel calculator and R script (available in the supplement, at GitHub, and Zenodo). These applications aim to support the harmonization of physiological parameter values and their associated variability for both sexes used in age-specific and lifetime PBK models.

### 2.2. Modification of existing age-specific PBK model to estimate lifetime mercury exposure – a case study

#### 2.2.1. Total mercury lifetime PBK model

We selected total mercury (Hg) exposure from diet as a case study because food is the primary source of chronic exposure (ANSES, 2011). To this end, the lifetime PBK model for total mercury was based on the structures and parameters from various published age-specific PBK models (Abass et al., 2018; Carrier et al., 2001; Gastellu et al., 2024; Ou

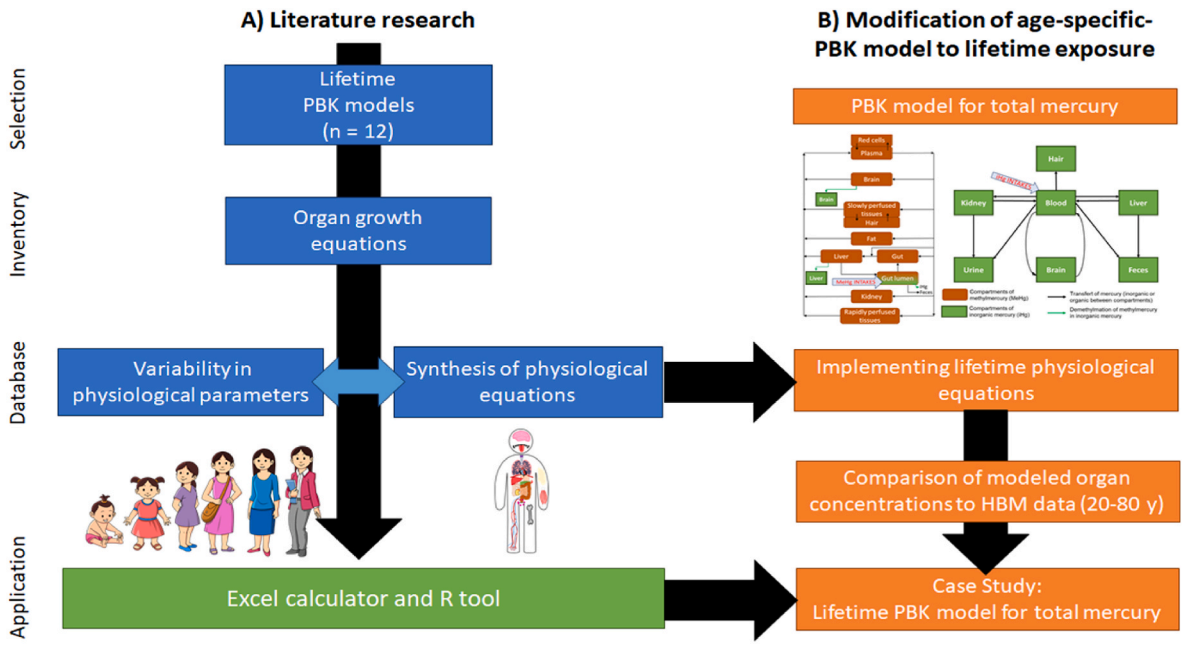


**Fig. 1.** The general workflow consisted of A) literature research of lifetime PBK models that originally applied physiological equations of organ growths and B) the modification of two age-specific PBK models of methylmercury and inorganic mercury to simulate total mercury over life. This workflow is suggested to improve dietary exposure assessment for chronic exposures.

**Table 1**
Overview of the 12 lifetime PBK models included in our study from which physiological equations describing volume changes of organs were extracted.

| Model sources | Substance family | Substances | Compartments | Routes of exposure |
|---|---|---|---|---|
| Beaudouin et al. (2010) (accounting pregnancy) | Environmental contaminants | 1,3-butadiene<br>2,3,7,8-tetrachlorodibenzo-p-dioxin (TCDD) | 22 | Ingestion, Inhalation |
| Deepika et al. (2021) | PFAS | PFOS | 10 | Ingestion |
| Haddad et al. (2001) | Non-specific family | Non-specific substance | 16 | |
| Haddad et al. (2006) | Volatile Organic Compounds<br>Disinfection by-products | Trichloroethylene<br>Trihalomethanes<br>Chloroform<br>Bromodichloromethane<br>Dibromochloromethane<br>Bromoform | 6 | Ingestion, inhalation, dermal |
| Mallick et al. (2020) | Pesticides (pyrethroids) | Deltamethrin<br>Cis-permethrin<br>Trans-permethrin<br>Esfenvalerate<br>Cyphenothrin<br>Cyhalothrin<br>Cyfluthrin<br>Bifenthrin | 7 | Ingestion, Inhalation |
| Pendse et al. (2020) | Non-specific family | Trichloroethylene<br>ATRA<br>Coumarin | 10 | Ingestion, Inhalation, Dermal, Intravenous |
| Price et al. (2003) | Volatile Organic Compounds | Furan | 17 | Inhalation |
| Ring et al. (2017) | Non-specific family | Non-specific substance | 17 | Ingestion |
| Sarigiannis et al. (2020) | Non-specific family | Bisphenol A<br>Bis(2-ethylhexyl)<br>DEHO<br>Cadmium | 14 | Ingestion, Inhalation, Dermal (pregnancy) |
| Smith et al. (2014) | Pesticides (and metabolites) | Chlorpyrifos<br>Chlorpyrifos-oxon (metabolite)<br>TCP (metabolite) | 15 | Ingestion |
| Verner et al. (2008) (accounting pregnancy) | Persistent Organic Pollutants (POP) | Hexachlorobenzene<br>PCB-153<br>PCB-180 | 10 | Ingestion |
| Wu et al. (2015) | PFAS | PFOA, PFOS | 5 | Ingestion |

et al., 2018; Pope and Rand, 2021). Fig. 2 illustrates the structure of two combined PBK models for MeHg and iHg to model the total mercury body burden as a mixture. Briefly, the PBK model for MeHg was adapted from Ou et al. (2018) and included 11 compartments. The PBK model published by Carrier et al. (2001) modeled the distribution of iHg. In the lifetime PBK model established here, both iHg and MeHg were connected by the demethylation of MeHg into iHg, enabling the calculation of total mercury. MeHg and iHg intakes were assumed to originate

**Table 2**

Summary of the original publications used to parameterize lifetime physiological equations for 24 tissues/organs extracted from the 12 lifetime PBK models. Body surface area is used as input in multiple physiological equations. All equations and original publications are documented in the Excel file (Supplement).

| | Haddad et al. (2001) | Price K. et al. (2003) | Haddad et al. (2006) | Verner et al. (2008) | Beaudouin et al. (2010) | Smith et al. (2014) | Ring et al. (2017) | Wu et al. (2015) | Mallick et al. (2019) | Pendse et al. (2020) | Sarigiannis et al. (2020) | Deepika et al. (2021) |
|---|---|---|---|---|---|---|---|---|---|---|---|---|
| Adrenals | | | | | **19** | | | | | | | |
| Blood | **1, 18, 28** | *15* | | | **19** | **41** | 3 | **9** | **9** | **9** | **19** | |
| Bone | **18** | *15* | **16**, 33 | | **19** | | **2, 21, 24** | | | | **19** | |
| Brain | **18** | *15* | | | **1** | **19, 25, 41** | **31** | | **38** | **38** | **19** | *32* |
| Breast | | | | 13 | **19** | | | | | | | |
| Body Surface Area | | | **14** | *16* | | | **17**, 36 | **12** | **12** | **12** | | **10** |
| Cardiac output | | **5**, 35 | 34 | *16* | **19, 25** | | | **8, 12** | *39* | **8** | | *27* |
| Diaphgram | | | | | | **4, 24** | | | | | | |
| Fat | **11, 30** | *15* | **16** | *16* | | **19, 41** | | **6** | **6** | **6** | **19** | *32*, **35** |
| Gonads | **1** | *15* | | 13 | **19** | | | | | | **19** | |
| Heart | **1** | *15* | 33 | *16* | **1** | | | | | | **19** | |
| Hematocrit | | | | | | | | **40** | **40** | **40** | **19** | |
| Intestine / Gut | **18** | *15* | | | **19** | **4** | | 33 | 33 | 33 | **19** | |
| Kidney | **1** | *15* | | | **1** | **41** | **31** | **14** | | 3 | **19** | **19** |
| Liver | **1** | *15* | **33** | *16* | **1** | **19, 25, 41** | **31**, 33 | **19** | **29** | **29** | **19** | *32*, **35** |
| Lung | **1** | *15* | | | **19** | **41** | **31**, 33 | | | 3 | **19** | *32*, **35** |
| Marrow | **18** | *15* | | | **19** | **4** | | | | | | |
| Muscle | **18** | *15* | | *16* | **19, 25** | **19**, 20, **25**, **41** | **40** | | | | **19** | |
| Pancreas | | | | | **19** | **4, 41** | **31**, 33 | | | | | |
| Plasma | | | | | | | | **9** | **9** | **9** | | |
| Red Blood Cells | | | | | | | | | | | | |
| Skin | **18** | *15* | 33 | *16* | **19** | **41** | 3 | | | 7 | **19** | |
| Spleen | **1** | *15* | | | **1** | **41** | **31**, 33 | | | | | |
| Stomach | **18** | *15* | | | **19** | | | | | | | |
| Thyroid | | | | | **19** | | | | | | | |
| Tongue | | | **33** | *16* | | | | | | | | |

Sources:

| | | | |
|---|---|---|---|
| 1 | Altman and Dittmer 1962 | 22 | Lafortuna et al. 2005 |
| 2 | Baxter-Jones et al. 2011 | 23 | Lexell et al. 1988 |
| 3 | Bosgra et al. 2012 | 24 | Looker et al. 2009 |
| 4 | Brown et al. 1997 | 25 | Luecke et al. 2009 |
| 5 | Cayler et al. 1963 | 26 | Luisada et al. 1980 |
| 6 | CDC 2014 | 27 | Mallick et al. 2019 |
| 7 | Clewell et al. 2004 | 28 | Morse et al. 1947 |
| 8 | Cowles et al. 1971 | 29 | Noda 1997 |
| 9 | Cropp 1971 | 30 | NRC 1993 |
| 10 | Du Bois and Du Bois 1989 | 31 | Ogiu et al. 1997 |
| 11 | Fomon et al. 1982 | 32 | Price K. et al. 2003 |
| 12 | Gehan and Georges 1970 | 33 | Price, P.S. et al. 2003 |
| 13 | Gentry et al. 2002 | 34 | Sholler et al. 1987 |
| 14 | Gilja, 1995 | 35 | Stader et al. 2019 |
| 15 | Haddad et al. 2001 | 36 | Verbraecken et al. 2006 |
| 16 | Haddad et al. 2006 | 37 | Webber and Barr 2012 |
| 17 | Haycock 1978 | 38 | Willmann et al. 2007 |
| 18 | ICRP 1975 | 39 | Wu et al. 2015 |
| 19 | ICRP 2002 | 40 | Yip et al. 1984 |
| 20 | Janssen et al. 2000 | 41 | Young et al. 2009 |
| 21 | Koo et al. 2000 | | |

Legend:

**i**: Equation refined on human data

*i*: Equation developed by a previous model

i: Equation validated with an existing model

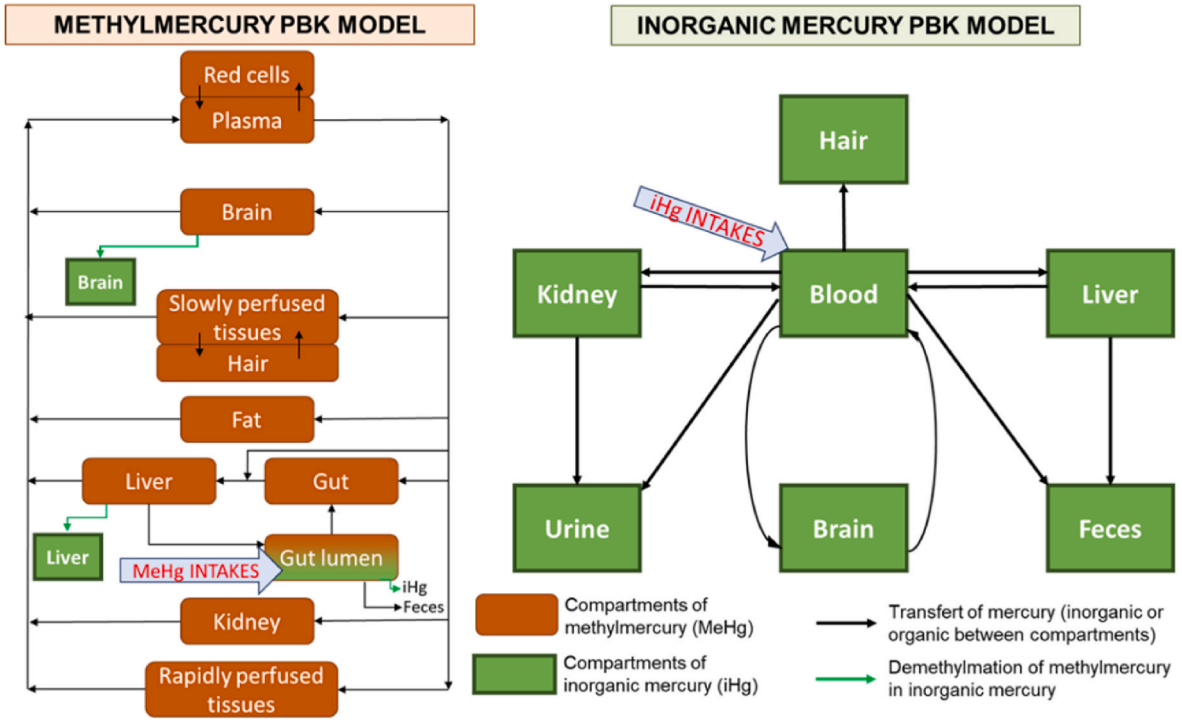


**Fig. 2.** Established PBK model of total mercury as combined methylmercury and inorganic mercury exposure. The left PBK model includes 11 compartments to simulate methylmercury (orange boxes) and the right PBK model consists of seven compartments to simulate inorganic mercury (green boxes) distribution throughout the body. The PBK model structures were adapted from Ou et al. (2018) for methylmercury and from Carrier et al. (2001) for inorganic mercury.

exclusively from dietary exposures (Kim et al., 2016). Specifically, MeHg intakes were integrated into the gut lumen and absorbed iHg doses were integrated in the blood as proposed by Abass et al. (2018) and Nuttall (2004), respectively. The diffusion of MeHg in the brain followed the model proposed by Pope and Rand (2021), who excluded the blood-brain barrier and thereby showed improved estimations compared with HBM data. In the PBK model for MeHg, the 'slowly perfused organs' compartment lumped skin, heart, diaphragm, muscles, bones, and marrow. The 'rapidly perfused organs' compartment lumped the thyroid, breast, lung, stomach, spleen, pancreas, adrenals, and gonads. Excretions of total mercury were simulated as the sum of iHg and MeHg concentrations in urine and hair, which are the main exposure biomarkers collected in HBM studies and usually measured as total mercury (Esteban-López et al., 2022). All mercury-specific model parameters are detailed in the Supplement (Section d).

We replaced the scaling factors of organ volumes used in the age-specific PBK models with physiological equations of organ growth (see section 2.2.1). As input for the physiological equations, body growth over a lifetime (body weight and height) was scaled on the French population (ANSES, 2017; Gastellu et al., 2024). Arithmetic means of body weight and height were computed separately for both sexes, using data from 5855 individuals aged from birth to 80 years.

#### 2.2.2. Construction of a virtual population with lifetime exposure trajectories

Mercury dietary exposure was performed using the lifetime exposure trajectory methodology based on French survey data. This methodology has been developed to construct chemical exposure throughout the lifetime considering five socio-economic and socio-demographic parameters (i.e., sex, age, region of habitation, body mass index, socio-economical index) of individuals with a coherent evolution from birth to 80 years. Trajectories were constructed for a pool of 500 virtual individuals to simulate the dietary exposure for a French representative population (Pruvost-Couvreur et al., 2020b, 2021). Real-measured dietary exposures were imputed for each day of the virtual individuals, considering the socio-demographic and socio-economic characteristics to model daily mixture intakes of iHg and MeHg (Gastellu et al., 2024). Individual dietary exposures were estimated based on the exposure data from the last Total Diet Studies (TDS) performed in France: TDS2 for the population from 3 to 80 years (ANSES, 2011). A specific TDS for infants under 3 years evaluated non-breastfeed consumption during childhood (ANSES, 2016). The food contamination data were reported in the CALIPSO study, which focused on monitoring seafood items (AFSSA, 2006). This data addition avoids underestimating the exposure to mercury by seafood. To finally estimate the daily exposure to MeHg and iHg for each individual (μg/kg bw/day), MeHg and iHg contamination data in different food items (j in μg/g) were combined with daily food consumption data (i in g/day) representative for the French population according to

$$Exposure = \frac{\sum^{l} i_l \times j_{Hg,l}}{Body\ weight} \qquad \text{Equation 1}$$

where l represents the different food and individual body weight (in kg). However, only total mercury was quantified in the French TDS, and the speciation hypothesis was therefore applied to estimate the speciation proportions of mercury in food products. Sirot et al. (2008) showed that MeHg is the dominant mercury form in seafood, while iHg is the dominant mercury form in other food products. More details on this methodology are available in a previous study (Gastellu et al., 2024).

### 2.3. HBM data of total mercury exposure

PBK model simulations were compared with real-measured concentrations of total Hg in different biological matrices (i.e., brain, kidney, liver, hair, and urine) from French HBM data (Bellouard et al., 2022; Goullé et al., 2010; Oleko et al., 2024) to refine and evaluate the lifetime PBK model. An overview of the studies is provided in Table 3. We hypothesized that exposure to mercury from food was constant over the past two decades, thereby allowing us to use the three HBM studies despite different sampling times of biological matrices.

**Table 3**
Description of HBM studies used to select or evaluate the lifetime mercury PBK model.

| Study | Number of individuals | Age of individuals | Analyzed matrices | Usage in this study |
|---|---|---|---|---|
| Bellouard et al. (2022) | 20 | 18–96 | Brain, Kidney, Liver, Hair | Selection |
| Goullé et al. (2010) | 21 | 19–57 | Brain, Kidney, Liver | Evaluation |
| Oleko et al. (2024) | 3471<br>1331 | 6–74 | Urine<br>Hair | Evaluation<br>Evaluation |

#### 2.3.1. HBM data set to select a set of physiological equations

The HBM data set published by Bellouard et al. (2022) was used with the purpose of selecting the best PBK model fit depending on the different sets of growth equations implemented for the modeled organs. Bellouard et al. (2022) reported concentrations of total mercury in several organs, including hair and urine, in addition to the ages of 20 individuals (Table 4). Urinary concentrations were not used in this study due to a limited number of samples (n = 6). The simulations of the modified lifetime PBK model for the virtual population were performed on only four sets of volume growth equations published by Haddad et al. (2001), Beaudouin et al. (2010), Smith et al. (2014) and Ring et al. (2017) due to calculation limits. These four sets of growth curves were selected because they had sex-dependent growth equations for at least five compartments in the mercury age-specific PBK model. Other equations extracted from the library described the organ growth of the lacking PBK compartments.

We evaluated the goodness of fit by comparing measured and simulated mercury concentrations for all organs. To this end, the simulations of the annual internal mercury concentrations in several matrices (i.e., brain, liver, kidney, and hair) were compared to the individual measurements at the corresponding ages (Bellouard et al., 2022). Between PBK model simulations, the physiological parameters were only modified according to the four sets of lifetime equations, while the chemical-specific parameters remained the same. For each tested PBK model, we determined a relative Root-mean-square error

**Table 4**
Distributions and coefficient of variations were used from Beaudouin et al. (2010) and McNally et al. (2014), respectively, to simulate the variabilities of organ growths in this study.

| Equations | Distribution | Coefficient of variation | |
|---|---|---|---|
| | | Male | Female |
| Bodyweight* | Normal | 0.15 | |
| Height* | Normal | 0.15 | |
| Brain | Normal | 0.05 | |
| Kidneys | Normal | 0.25 | |
| Liver | Normal | 0.24 | 0.25 |
| Pancreas | Normal | 0.27 | 0.29 |
| Stomach | Normal | 0.31 | |
| Intestine (small) | Normal | 0.12 | 0.13 |
| Intestine (large) | Normal | 0.20 | 0.14 |
| Heart | Normal | 0.19 | 0.25 |
| Bone | Normal | 0.01 | |
| Gonads | Normal | 0.05 | |
| Lungs | Log-normal | 0.33 | |
| Spleen | Log-normal | 0.38 | |
| Muscles | Log-normal | 0.27 | |
| Adipose | Log-normal | 0.42 | |

(RMSE) for the respective organ (k) as a goodness-of-fit metric, with weights proportional to the magnitude of errors. Then, an average of all the RMSE values was calculated in the same unit as the target variable (Eq. (2)) according to

$$RMSE_k = \sqrt{\frac{\sum \left(\frac{Hg_{Estimated} - Hg_{HBM}}{Hg_{HBM}}\right)^2}{N}} \quad \text{(Equation 2)}$$

with $Hg_{HBM}$ representing the total mercury concentrations (μg/g) measured in organ k for each individual (Bellouard et al., 2022), $Hg_{Estimated}$ is the average total mercury concentration (μg/g) in organ k estimated at each individual's age (Bellouard et al., 2022), and N is the number of individuals for which measurements in the respective organ exist. The different sets of physiological growth equations were implemented in the PBK model and RMSE was calculated for each simulation. The model associated with the lowest average RMSE was selected and further evaluated as the best lifetime PBK model for total mercury using two other HBM data sets as described below.

#### 2.3.2. HBM data sets to evaluate the total mercury lifetime PBK model

The selected lifetime PBK model was thereafter evaluated by comparing the variability of modeled mercury concentrations with measured exposure biomarkers from two HBM data sets (Goullé et al., 2010; Oleko et al., 2024). To this end, we ran the selected lifetime PBK model ten times by integrating population variability. Variability of organ volume was added to the established total mercury lifetime PBK model for each compartment as proposed by McNally et al. (2014). The variability of organ volume was computed by assuming either a normal distribution (Eq. (3)) or log-normal distribution (Eq. (4)) for the different organs, as listed in Table 4.

$$\Delta V_{Organ} = \sqrt{N(1, CV)^2} \quad \text{(Equation 3)}$$

$$\Delta V_{Organ} = \log(N(1, CV)) \quad \text{(Equation 4)}$$

The parameter $\Delta V_{Organ}$ represents the variability for the organ volume, (log) N is the (Log) Normal distribution, and CV means the coefficient of variation. Please note that the normal distribution is the squared root of the squared distribution to avoid negative values. The coefficient of variation for each organ and for both sexes is detailed in Table 4.

Goullé et al. (2010) measured concentrations of total mercury in the brain, kidney, and liver from autopsied adult people but without reporting the ages of the individuals (Table 3). Therefore, those measured organ concentrations were used to evaluate the distributions in respective organs gained from the selected lifetime PBK model simulated for our virtual adult population.

The Esteban population cohort was additionally used to evaluate the selected lifetime PBK model for total mercury on measured urine and hair concentrations in 4802 individuals (6–74 years old) (Oleko et al., 2024). Biomarkers were sampled in France between 2014 and 2016. The average and 95$^{th}$ percentile total mercury concentrations measured in hair and urine obtained for different age groups of the Esteban participants were compared to simulated population distributions of mercury in exposure biomarkers at different stages of life, including childhood.

### 2.4. Risk assessment of lifetime exposure to mercury

We aimed to illustrate how to refine risk characterizations and support regulatory decisions by using the established PBK model as a lifetime exposure trajectory methodology. Using a statistical approach, we first correlated annually averaged biomarker concentrations estimated by the lifetime PBK model with the real-life exposures to MeHg and iHg intakes combined for each year of life. Pearson's correlation with statistical significance of $p \leq 0.05$ was used to identify associations between intakes of the two mercury forms and exposure concentrations in hair, urine, and organs. This information is important for refined risk assessment.

We also translated maximum levels in seafood items, tolerable MeHg and iHg intakes defined for populations (HBGV), and real intakes to total mercury estimated in hair and urine using the selected lifetime PBK model. Hereby, maximum contamination levels for total mercury in salt, food supplements, and seafood products are regulated to limit the exposure and are currently set at 0.1 mg/kg wet body weight of salt and food supplements as well as 0.3, 0.5, and 1.0 mg/kg wet body weight of fishery products, muscle meat of fish, and crustaceans in accordance with European Commission Regulation (EU) 2023/915B. Please note that we only simulated the three highest maximum contamination limits with a focus on seafood consumption as a main source of MeHg intake (Sirot et al., 2008). In addition, we used weekly tolerable intakes for iHg and MeHg to estimate total mercury in urine and total mercury in hair, respectively, representing the most robust biomarker for each mercury form Oleko et al. (2024). To this end, 11.5 mg/kg of MeHg in maternal hair was associated with neurodevelopment effects identified in children and foetus as the critical effect based on epidemiology studies (EFSA, 2012). This point of departure corresponds to the intake of 1.3 μg MeHg/kg body weight/week defined as HBGV. For iHg, the weekly intake of 4 μg iHg/kg body weight is defined as HBGV, considering a renal effect. Please note that the HBGV considers the critical effect to be triggered by the same concentration of only one chemical at all stages of life. At the same time, our lifetime PBK model simulates total mercury as a mixture of MeHg and iHg linked to different effects.

### 2.5. Software and codes

All calculations were made with the software R (v.4.2.3). The R package '*mrgsolve*' (v.1.4.1) was used to code the models and to solve the differential equations of PBK models (Baron et al., 2022). To this end, we conducted forward simulations based on reported PBK parameter values and variability estimates of exposure intakes and organ volumes as described earlier. The code of the total mercury PBK model and all lifetime physiological models are available on a GitHub repository and Zenodo with an example of lifetime exposure trajectories to MeHg and iHg. An Excel file and an R code provide all the equations of lifetime physiological models calculating the volume of organs for all stages of life after birth (Supplement).

## 3. Results and discussion

### 3.1. Database of lifetime PBK models and their physiological equations

Twelve PBK models simulated internal exposure over a lifespan for various chemical classes, e.g., pesticides, persistent organic pollutants, or volatile organic compounds (Table 1). The PBK models contained between five (Wu et al., 2015) and 22 compartments (Beaudouin et al., 2010). Information on compartments and corresponding lifetime equations from reviewed PBK models were extracted for both sexes to create a library of organ-specific lifetime equations. This inventory illustrated that multiple equations have been developed over the last decades to describe the growth of major organs (i.e., liver, kidney, brain) and other physiological parameters. In total, 24 physiological parameters were identified, covering the volume growth of major organs, cardiac output, hematocrit, and body surface area (Fig. 3). Different equations were extracted from the reviewed literature to simulate organ growths as a function of different body parameters (weight, height, or body surface area). The number of different lifetime equations per organ ranged from one equation for the thyroid, diaphragm, and adrenal glands to 12 equations for the liver (Fig. 3). Moreover, two or three separate equations described some lifetime growth equations to model different dynamics of volume growth as a function of age. All equations have been compiled and are prepared for calculating age-specific organ volumes as

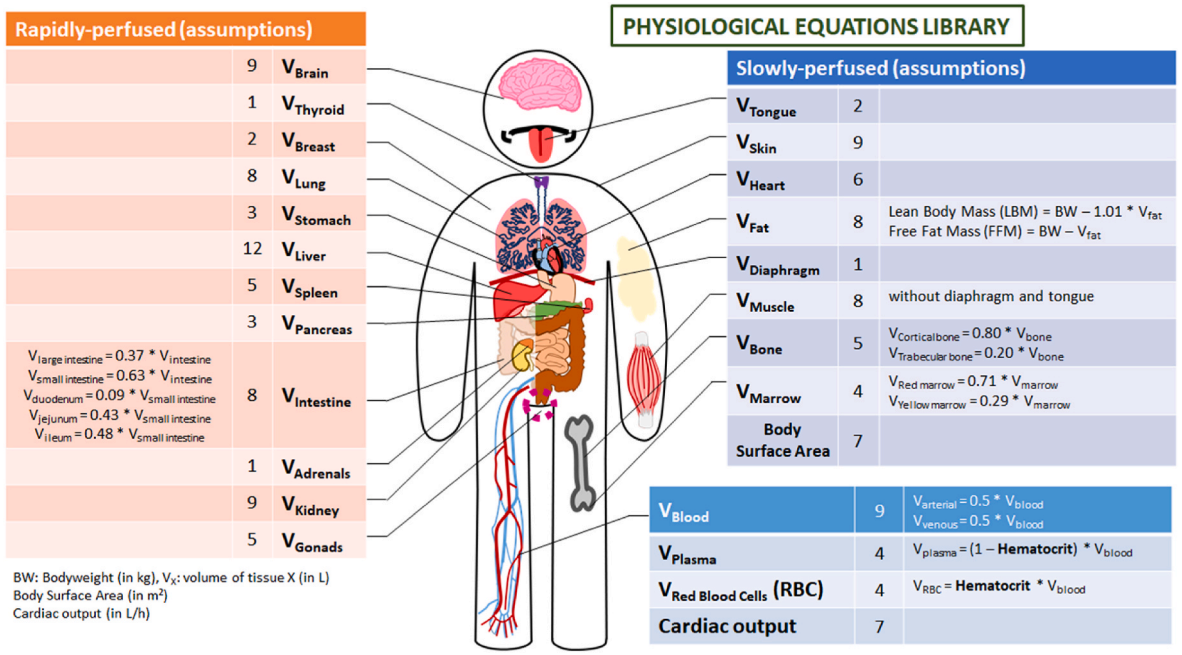


**Fig. 3.** Total number of physiological equations per organ identified in the 12 different lifetime PBK models that were used to simulate volume growth (V). Equations for `rapidly perfused organs' and 'slowly perfused organs' are found in the lifetime physiological equation library (Excel file in the Supplement). The number of equations identified per organ is detailed in the central column of the table. In addition, we assumed a constant rate throughout the lifetime to calculate the volume of organs for which no physiological equations existed (e.g., intestine, fat, bone, marrow) as reported by Brown et al. (1997).

well as the lifetime growth of organ volumes (Excel and R files in Supplement and GitHub repository/Zenodo).

No physiological equations existed for a few organs/tissues (e.g., intestine, fat, bone, marrow). Instead, constant rates were applied as reported by Brown et al. (1997) to model growth over a lifetime (Fig. 3). Interestingly, physiological equations describing the evolution of the blood flow to organs over a lifetime were applied in only a few lifetime PBK models, such as blood flow to the brain (Price et al., 2003) and other organs (Sarigiannis et al., 2020) (Excel file in the Supplement). Given the limited selection of lifetime equations, we applied constant rates

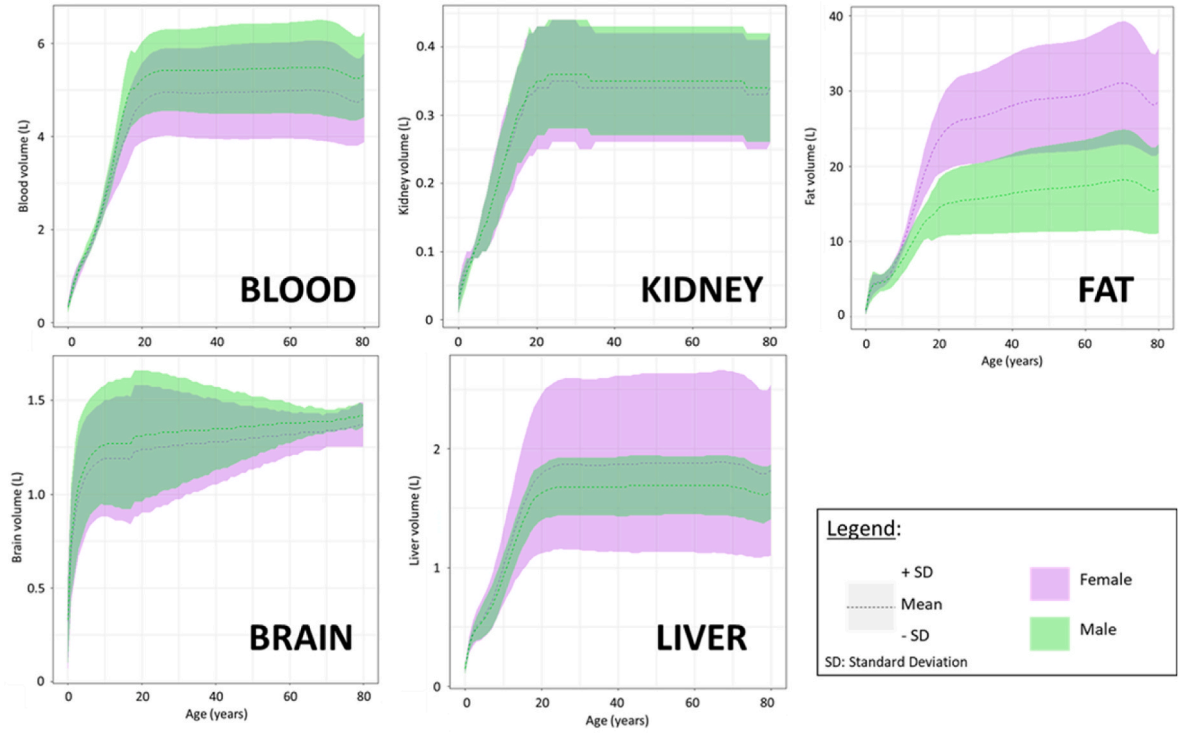


**Fig. 4.** Graphical representation of the volume growth variability for major organs (e.g., blood, kidney, fat, brain, and liver, in L) over time (years) depending on the different lifetime physiological equations. The dashed curves represent the average volume growth based on all physiological equations. The colored areas represent the standard deviation values. The variability is indicated for both sexes. The growth curves of other organs are depicted in the Excel file (Supplement).

relatively scaled to the growth of organ volumes for the blood flow to each organ as proposed by Beaudouin et al. (2010).

### 3.2. Variability in organ growths

The shapes of the growth curves for the same organs were similar between the different physiological equations (Fig. 4). Commonly, organ volumes increased over approximately 18 years of age until reaching a plateau. Some modeled organ volumes fluctuated after 18 years of age due to body weight and height variations (Excel file and R code in Supplement). The coefficient of variations (CV) resulting from the different physiological models ranged between ~10% and <90%, with <30% variability usually estimated for the organs most frequently used in age-specific PBK models, including blood, liver, kidney, muscles, and lungs (Excel sheet in supplement). The variation in organ volumes aligned well with the CV values reported by McNally et al. (2014) (Table 3). It is important to note that variation differs between life stages, with generally higher variation observed during infancy, toddlerhood, and in adults over 60 years of age. The higher variation may be attributed to the limited data available for calibrating physiological lifetime equations at early and late life stages.

Multiple factors might contribute to variability in organ growth over a lifetime. Firstly, differences in growth curves between identified lifetime physiological models likely reflect population variability, including differences in race and ethnicity (Ring et al., 2017). Secondly, lifetime physiological equations were derived from different body parameters such as age, body weight, or height. Thirdly, polynomial equations might differ, resulting in different estimated parameters from the regression to a similar or even identical data set of organ volume measurements. For example, the PBK models established by Beaudouin et al. (2010) and Sarigiannis et al. (2020) used ICRP (2002) data to fit growth curves differently. Fourthly, the authors might not have considered the same tissues for a common biological term. Fat, for instance, can also be designed as adipose tissue. These terms may consider overall adipose tissues or only the non-essential adipose tissues (Price et al., 2003). This issue needs better descriptions of the physiological parameters with a common language between PBK models (Ruebenacker et al., 2007). Due to the strong need within the scientific community for a PBK ontology, efforts should be made to develop and standardize such a framework. Lastly, some equations were calibrated for a limited age range, and additional uncertainty was introduced when volume growth was extrapolated to other age groups. For instance, Haddad et al. (2001) developed growth curves for multiple organs based on a data set published by Altman and Dittmer (1962), who reported organ weights gained from birth to 18 years of age.

### 3.3. Sex-dependent organ growths

The dynamics of organ growth as a function of sex have been described differently. One lifetime PBK model analyzed male individuals only (Price et al., 2003) and two PBK models females (Verner et al., 2008; Wu et al., 2015). Nine out of 12 PBK lifetime models reported physiological lifetime equations for both sexes, highlighting the importance of considering sex-specific physiological growth curves in lifetime PBK models. Five of these models considered the same coefficients of the polynomial equations, thus introducing differences in organ growth through sex-specific body parameter dynamics as input to the growth equations (Haddad et al., 2006; Mallick et al., 2020; Pendse et al., 2020; Sarigiannis et al., 2020; Smith et al., 2014). The other four PBK models applied sex-specific physiological equations and sex-specific body parameters for most organs (Beaudouin et al., 2010; Deepika et al., 2021; Haddad et al., 2001; Ring et al., 2017). Fig. 4 illustrates the volume curves of major organs for both sexes. Naturally, sex-specific physiological equations might reflect better physiological differences between sexes to consider the variability as a potential source for chemical body burden differences. However, it should be noted that variability may be more accurately estimated in organs where a greater number of physiological equations exist compared to those organs that are underrepresented in PBK models due to limited data (Fig. 3).

### 3.4. Modification of an age-specific PBK model to lifetime mercury exposure

Daily exposures to MeHg and iHg were estimated based on French consumption and food contamination levels (Eq. (1)). These individual lifetime exposure trajectories were input in the lifetime PBK models. Simulation results on populational lifetime dietary exposure to MeHg and iHg are provided in supplementary material (Figs. S2 and S3). Three different HBM data sets were used to compare the PBK simulations for total mercury with concentrations measured in French individuals (Table 4). Hence, the following PBK simulations were solely based on the French population, including body growth parameters, dietary exposure trajectories, and measured internal mercury concentrations.

#### 3.4.1. Selection of physiological lifetime equations implemented in the mercury PBK model

The HBM data set from Bellouard et al. (2022) was used to select the best-fitting physiological lifetime equations implemented in the mercury PBK model, based on total mercury measurements in autopsied organs of 20 individuals. As shown in Fig. 5, the highest mercury concentrations were measured in hair, followed by kidney and liver, regardless of age, which aligns with our simulations. Measured mercury concentrations increased over age in all sampled organs, specifically after age 60. Lower mercury concentrations in younger generations might reflect successful risk management strategies to decrease mercury exposure, such as recommendations for seafood consumption (i.e., seafood type and frequency), which have been communicated to the general population to increase overall awareness and prevent mercury-associated risks. In addition, encapsulated amalgams have been replaced by composite resins (Basu et al., 2018). However, this trend needs to be interpreted cautiously as fewer total mercury measurements were retrieved from autopsy samples before the age of 60 and the limited number of individuals might have reduced the robustness of the variability.

Four sets of volume growth equations were implemented in the mercury PBK model and the average RMSE was calculated for hair, kidney, liver, and brain. The average calculated RMSE values ranged between 0.81 with the equation set extracted from Beaudouin et al. (2010) as the best fit and 0.89 with the equation set extracted from Haddad et al. (2001) as the worst fit. Thus, the physiological equations extracted from Beaudouin et al. (2010) were selected and implemented in the lifetime PBK model, which was further complemented with volume equations for adipose tissue (Deepika et al., 2021), bones (Ring et al., 2017), and hematocrit (Mallick et al., 2020), considering the lowest RMSE.

The lifetime PBK model simulated an increase in average mercury concentrations in hair, kidney, brain, and liver during childhood due to the onset of early consumption of seafood and fatty fish, and remained stable after 25 years of age (Fig. 5). Basu et al. (2018) reported that adults had blood mercury concentration around twice those found in children according to their meta-study, which also reflects the increase in mercury body burden between childhood and adulthood (ATSDR, 2022). The discrepancy between individual mercury measurements and simulated average concentrations became more pronounced after the age of 60, with liver and hair concentrations underestimated in the elderly. This underestimation of total mercury in the elderly could be due to higher seafood consumption or the presence of dental amalgams. Both factors were not considered in this lifetime PBK model.

#### 3.4.2. Evaluation of the established lifetime mercury PBK model

HBM data reported by Goullé et al. (2010) and by Oleko et al. (2024) were further used to evaluate the fits by the established lifetime PBK model.

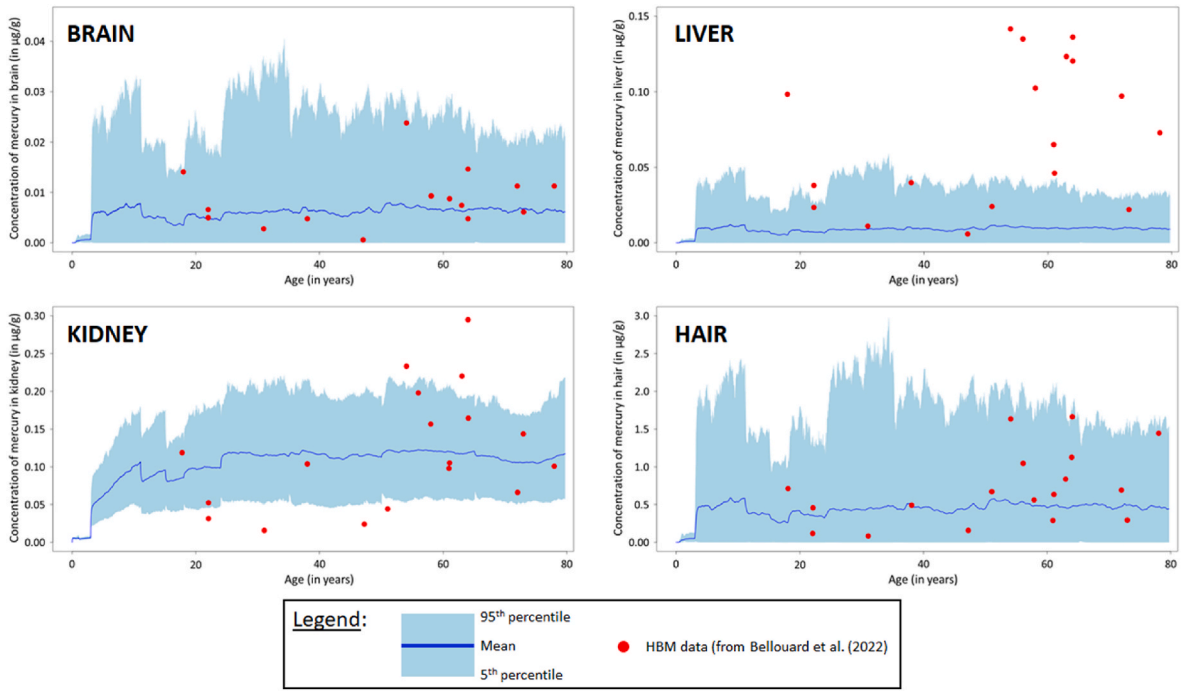


**Fig. 5.** Simulated total mercury concentration over life in different human matrices (hair, kidney, brain, and liver) using the selected lifetime PBK model with the set of physiological equations extracted from Beaudouin et al. (2010). The bold line represents the average modeled concentration, and the blue bands represent the population distribution between the 5th and 95$^{th}$ percentile. The red dots show the measured total mercury concentrations published by Bellouard et al. (2022).

*3.4.2.1. HBM data from Goullé et al. (2010).* Firstly, the lifetime PBK model was evaluated using total mercury measurements in the brain, kidney, and liver from 21 autopsied individuals of unknown ages (Goullé et al., 2010). Here, the same exposure scenarios were simulated as before, but organ volume variability was added to simulate population variability (Table 4). The average simulated brain and kidney concentrations agreed well with the average total mercury measurements in the respective organs (Table 5). However, the average liver concentration was underestimated by 7.4 times compared to the measured mean concentration, likely because the liver does not accumulate mercury in the same way as the kidney accumulates iHg. Moreover, the imputation methodology likely underestimated the exposure to MeHg among low seafood consumers (Gastellu et al., 2024), which may be an additional factor contributing to the overall underestimation. Advanced methodologies could be used, such as the method developed by the National Cancer Institute (NCI) or the Multiple Source Method (MSM) to integrate consumption data frequency and refine mercury exposure assessment (Harttig et al., 2011; Tooze et al., 2006). A drawback of these imputation methodologies is, however, that they extrapolate only one chemical and not the mixture of iHg and MeHg. New developments are therefore necessary to estimate the distribution of the internal exposures more accurately, particularly in the context of chemical mixtures.

**Table 5**
Comparison of the measured and simulated total mercury concentrations (in µg/g) in brain, kidney, and liver for adults. Total mercury concentrations reported by Goullé et al. (2010) are presented as average and 10th and 90th percentile ranges, while the simulated concentration is given as average in adults.

| | Brain | Kidney | Liver |
|---|---|---|---|
| Average concentration [10th percentile – 90th percentile] (Goullé et al., 2010) | 11.12 [4.14–20.41] | 119.97 [20.87–441.44] | 66.91 [12.39–170.36] |
| Average simulated concentration in adulthood | 6.2 | 115.1 | 9.0 |

*3.4.2.2. HBM data from Oleko et al. (2024).* Secondly, total mercury was measured as concentrations in hair and urine samples in the Esteban cohort (Oleko et al., 2024) (Table 6, Fig. 6). Importantly, exposures to MeHg and iHg reflect total mercury concentration measured in hair and urine, respectively (Oleko et al., 2024). Those concentrations might be influenced over life due to age-related factors such as body growth, dietary changes, and behavior changes (Gastellu et al., 2024).

*3.4.3. Urine concentrations - Esteban study (Oleko et al., 2024)*

The average total mercury concentrations measured in urine are almost constant over the age groups (Oleko et al., 2024). In contrast, simulated total mercury increased slightly in urine between childhood and adulthood and underestimated the average concentration by a factor of 2–3, but also could not reach the variability observed in the HBM data (Fig. 6). Even the estimations of the 95$^{th}$ percentile were underestimated by a factor of 5–7 regardless of the age group (Table 6). This result contrasts our findings that simulated total mercury in the kidney agreed well with measurements (Goullé et al., 2010), assuming that a high positive correlation ($R^2 = 1$) between estimated kidney and urine concentration exists (Fig. 7). This high correlation was also found by Esteban-López et al. (2022). A consequent hypothesis would be that mercury in urine might have originated from iHg exposures by ingestion and inhalation, which we would have underestimated due to the lack of information on individual exposures from smoking, environmental pollution (natural or industrial for those living close to an industry releasing iHg in the atmosphere), and dental amalgams (Oleko et al., 2024). Moreover, the lifetime PBK modeling estimates an average daily concentration in urine, while total mercury concentration measurements represent concentrated mercury from first-morning urine. Altogether, total mercury measurements in urine were associated with high uncertainties in our estimates, which was also reflected in the data discussed by Esteban-López et al. (2022). Notably, the contribution of iHg to total mercury estimated in urine accounted for around 90, according to the PBK model results (Fig. S4).

**Table 6**
Comparison of total mercury concentrations in urine (μg/L) and hair (μg/g) measured in Esteban (Oleko et al., 2024) and the mean and 95th percentile interval (standard deviation) estimated by the lifetime PBK model. (Urine: LOD = 0.012 μg $L^{-1}$, LOQ = 0.04 μg $L^{-1}$; Hair: LOD = 0.005 μg/g, LOQ = 0.012 μg/g).

| | | | 6–10 years | 11–14 years | 15–17 years | 18–29 years | 30–44 years | 45–59 years | 60–74 years |
|---|---|---|---|---|---|---|---|---|---|
| **Urine** (μg/L) | Nr of HBM samples | | 477 | 389 | 186 | 161 | 609 | 893 | 756 |
| | Mean | HBM data | 0.92 [0.82; 1.02] | 0.85 [0.77; 0.94] | 0.96 [0.82; 1.13] | 0.63 [0.48; 0.84] | 0.96 [0.85; 1.09] | 0.74 [0.65; 0.84] | 0.62 [0.55; 0.70] |
| | | PBK model | 0.3 | 0.3 | 0.3 | 0.4 | 0.4 | 0.4 | 0.4 |
| | 95th percentile | HBM data | 3.07 [2.41; 4.77] | 2.84 [2.26; 3.23] | 2.96 [2.58; 3.17] | 3.28 [2.59; 4.69] | 4.15 [3.57; 4.65] | 3.07 [2.62; 3.66] | 2.57 [2.29; 2.85] |
| | | PBK Model | 0.5 | 0.5 | 0.5 | 0.6 | 0.7 | 0.7 | 0.6 |
| **Hair (μg/g)** | Nr of HBM samples | | 239 | 223 | 108 | 47 | 190 | 268 | 256 |
| | Mean | HBM data | 0.37 [0.31; 0.44] | 0.27 [0.22; 0.34] | 0.29 [0.21; 0.42] | 0.49 [0.35; 0.68] | 0.50 [0.41; 0.61] | 0.69 [0.60; 0.79] | 0.69 [0.60; 0.81] |
| | | PBK model | 0.5 | 0.4 | 0.3 | 0.4 | 0.5 | 0.5 | 0.5 |
| | 95th percentile | HBM data | 1.33 [0.99; 1.80] | 0.97 [0.76; 1.21] | 1.00 [0.70; 1.31] | 2.50 [1.33; 5.15] | 1.92 [1.54; 3.20] | 2.21 [1.77; 2.40] | 2.36 [1.82; 3.59] |
| | | PBK Model | 1.9 | 1.4 | 1.0 | 1.7 | 1.9 | 1.8 | 1.6 |

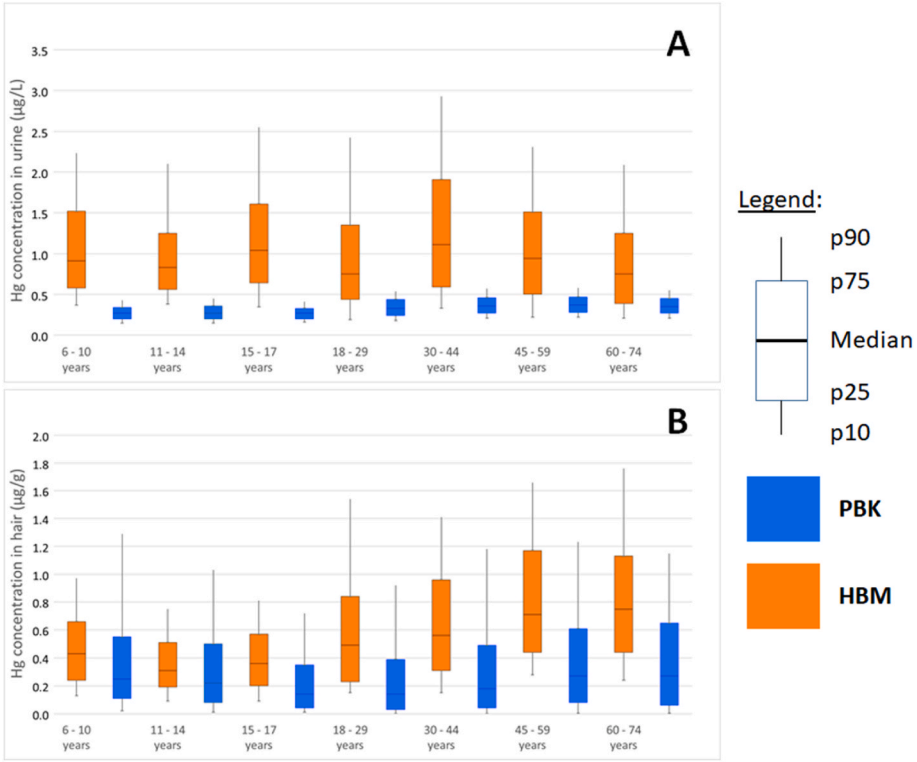


**Fig. 6.** Simulated concentration of total mercury in (A) urine and (B) hair using the selected lifetime PBK model with the set of physiological equations extracted from Beaudouin et al. (2010) (in blue) compared to the Esteban data (in orange) reported by Oleko et al. (2024). The bars represent population distributions, illustrating the median, 25th-75th percentiles, and 10th-90th percentiles.

*3.4.4. Hair concentrations - Esteban study (Oleko et al., 2024)*

The total mercury concentration in hair is considered a robust biomarker of exposure to MeHg, originating mainly from seafood (Sirot et al., 2008). The distributions of total mercury concentration measured in hair from the Esteban study were compared to the simulated hair exposures for different age groups (Table 6, Fig. 6). Total mercury concentrations measured in hair from the Esteban participants slightly decreased during childhood, likely caused by dilution effects due to the body growth. Afterward, mercury concentrations in hair increased during adulthood, likely due to higher consumption of seafood, particularly fatty fish and crustaceans (Oleko et al., 2024). In addition, the variability became larger with the increasing ages of the Esteban participants. The lifetime PBK model also simulated the dynamic of the HBM data in dependence on age. Specifically, improved fits of mercury concentration distributions in hair during childhood for the age groups 6–10 years and 11–14 years were performed (Gastellu et al., 2024). Considering the comparisons between the mean and the 95th percentile of HBM data and the simulated data, results are within the confidence interval of HBM data for some age groups of age (15–17, 18–29, 30–44, and 45–59 years of age). Moreover, differences between the estimated internal exposures and the HBM data were below a factor of 2, which is considered a well-established PBK model (WHO and IPCS, 2021). In

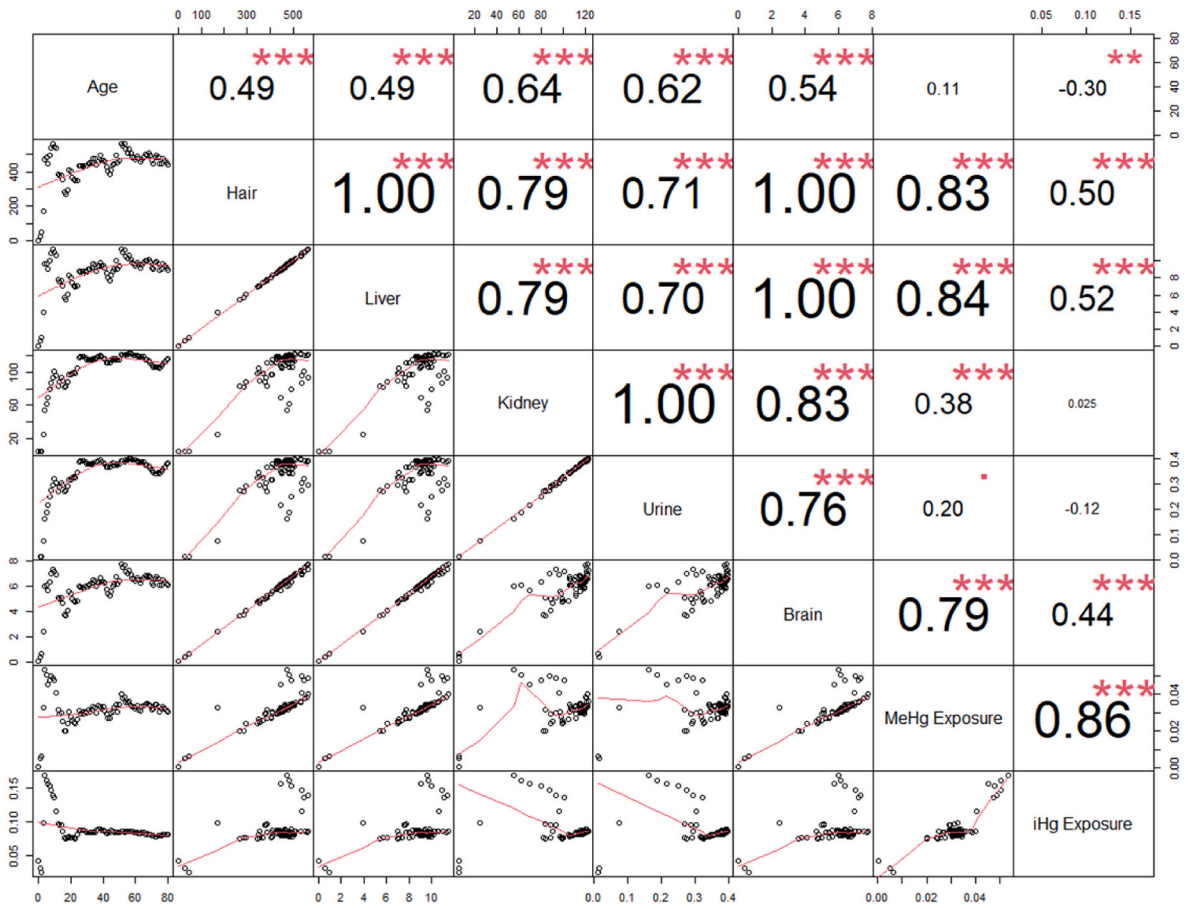


**Fig. 7.** Correlations of the average concentrations estimated by the lifetime PBK model for each year of life between different mercury biomarkers including MeHg and iHg intakes, concentrations in hair, urine, and in organs (liver, kidneys and brain), and age. The score of the Pearson correlation is shown on the right with p-value ("***": <0.001, "**": <0.01, "*": <0.05, ".": <0.1).

addition, the individuals with the highest mercury concentrations in hair were well estimated, even if the population distributions were underestimated. Therefore, the PBK model can be considered robust in estimating mercury concentration in hair over a lifetime. Thus, this methodology could be used in the risk characterization of a mixture (i.e., MeHg and iHg), which is considered an improvement compared with our previous PBK model without integrating lifetime physiological equations (Gastellu et al., 2024). Finally, only MeHg contributed to total mercury estimated in hair according to the PBK model results (Fig. S4).

### 3.5. Implications for mercury risk assessment

#### 3.5.1. Associations between exposures to both mercury forms and exposure biomarkers

The HBM data used provided various pieces of information to estimate real-life intake exposures to total mercury using organ doses or surrogate doses measured in urine and hair. However, the risk assessment for mercury is challenging because mercury forms can be differently abundant in hair and urine matrices, which is not well reflected by the total mercury measurements. We therefore sought to facilitate translation between external intakes and internal exposures of both mercury forms in our lifetime PBK model application by correlating MeHg and iHg intakes with total mercury concentrations in hair, urine, and target organs (Fig. 7). Total mercury concentration in hair was strongly correlated with concentrations in liver and brain, primarily reflecting exposure to MeHg (Oleko et al., 2024). These results support that the total mercury concentration in hair is a robust biomarker of exposure to characterize the risk of neurodevelopmental effects associated with MeHg exposure. In contrast, total mercury concentration in urine was highly correlated with concentrations in the kidney, illustrating iHg accumulation in this organ and its excretion via urine (Oleko et al., 2024). The total mercury concentration in urine is a better biomarker to characterize the risk of nephrotoxic effects associated with iHg exposure. To conclude, the PBK model provides a powerful tool for improving understanding of HBM data and refining dietary risk assessment by evaluating various biomarker measures.

#### 3.5.2. Estimation of mercury in hair and urine based on various intake scenarios

We further translated various regulative-relevant reference values for risk management to total mercury concentrations in hair and urine, the robust biomarkers for mercury often used in HBM studies. Fig. 8 shows the simulated mercury concentrations in hair and urine over a lifetime based on three intake scenarios: maximum mercury limits in seafood (considering only MeHg contamination in seafood), the HBGVs for MeHg and iHg, and realistic mercury intakes based on the French consumption data. In these simulations, we also accounted for population variability of consumption and physiological parameters to estimate likely concentrations between the median and the 95$^{th}$ percentile in hair and urine. Our simulations illustrated that extrapolated hair and urine concentrations fluctuate over time due to different seafood consumption patterns and body growth.

*3.5.2.1. Methylmercury.* As MeHg is the mercury form mainly contributing to hair exposure, we only simulated total mercury concentration in hair based on seafood consumption and compared estimated hair concentrations with the MeHg HBGV for refined risk assessment (Fig. 7).

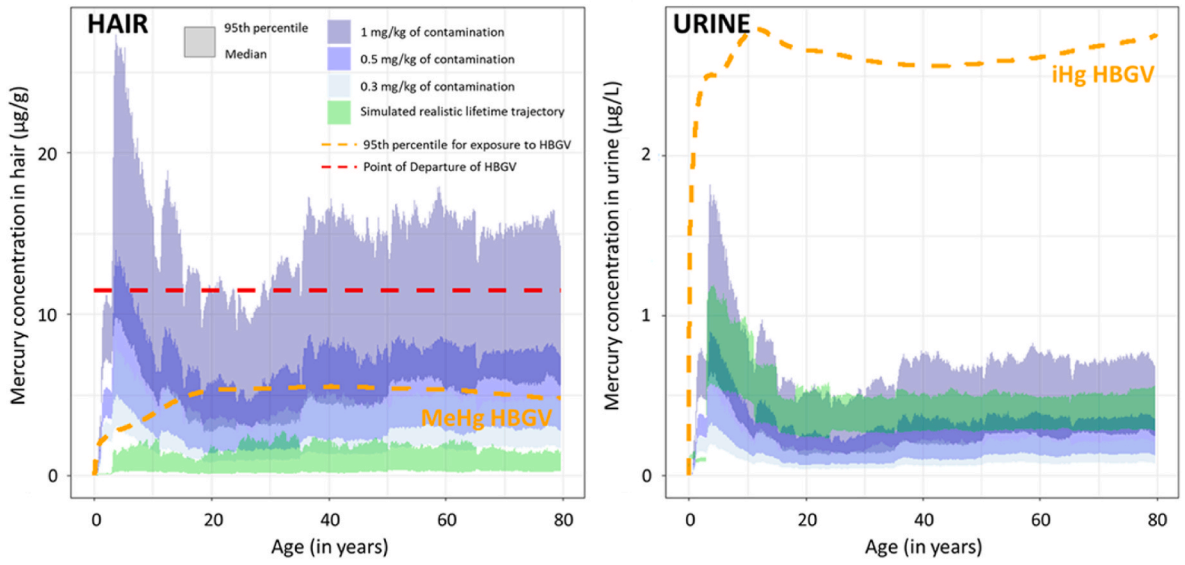


**Fig. 8.** Estimated total mercury concentration in hair (left) and urine (right) of a heterogenous population across all ages considering three intake scenarios: A) methylmercury contamination of 0.3 mg/kg (light blue), 0.5 mg/kg (blue), and 1 mg/kg (dark blue) wet bodyweight of all seafood items, B) a realistic simulated lifetime dietary exposure to total mercury according to the established lifetime PBK model (green) and C) the 95$^{th}$ percentile of constant exposures to MeHg HBGV (intake of 1.3 µg MeHg/kg body weight/week) and to iHg HBGV (intake of 4 µg iHg/kg body weight/week) (orange dotted lines). The variability of total mercury concentrations for each intake scenario ranges between median and 95$^{th}$ percentile estimates. The Point of Departure for neurodevelopmental effects associated with 11.5 mg/kg of total mercury in maternal hair (EFSA, 2012) is added as a red line.

Intake of 1 mg MeHg/kg contamination of seafood resulted in median mercury concentrations over 10 µg/g across nearly all ages, often reaching concentrations of 11.5 µg/g mercury in hair and higher for high seafood consumers, which would indicate an increased risk probability for neurodevelopmental effects (ATSDR, 2022). The 95$^{th}$ percentile of total mercury concentrations in hair on the basis of lower maximum mercury limits in seafood items as well as HBGV of MeHg was simulated to be mostly below its corresponding Point of Departure across all ages.

*3.5.2.2. Inorganic mercury.* As iHg is the mercury form mainly contributing to urine exposure, we only simulated total mercury concentration in urine based on seafood consumption and compared total mercury concentration in urine with the iHg HBGV for refined risk assessment (Fig. 8). Simulated total mercury concentrations in urine are close between intakes of 1 mg MeHg/kg contamination of seafood and realistic mercury intakes. It has to be noted that a fraction of iHg in urine results from demethylation of MeHg in the body according to the PBK model. Urine mercury concentrations estimated based on maximum levels of seafood contamination and realistic mercury intakes were around five times lower than the translated urine concentration based on iHg HBGV. However, the validation simulations described earlier showed that total mercury in urine were less well predicted as total mercury in hair (Fig. 6). Therefore, this refined risk estimation for iHg in urine has to be carefully interpreted considering high uncertainties like other exposure sources (i.e., inhalation, dental amalgam), which were not considered in the here performed intake calculations together with iHg formation in the body due to MeHg demethylation.

### 3.5.3. Childhood exposure

Early childhood exposure was found to be a critical exposure window due to the onset of seafood consumption combined with smaller body sizes, resulting in peak concentrations of mercury in hair before five years of age. Even 0.5 mg/kg mercury in seafood items could reach levels in hair close to the Point of Departure during early childhood. Nevertheless, mercury hair concentrations based on the simulated realistic lifetime trajectories to total mercury calculated from the Total Diet Studies were lower than the extrapolated hair concentrations based on maximum levels and MeHg HBGV. However, it has to be noted that our simulations were not validated with total mercury measurements in hair from children younger than six years of age (Table 6) and reported HBM data are rare for this subpopulation. McDowell et al. (2004) reported 0.22 µg/g as mean hair concentration in one to five years old children from USA. One-year-old children from the Faroe islands had on average 1.12 µg/g total mercury in their hair (Grandjean et al., 1997), and 4-years-old preschool children from Spain had 0.94 µg/g (Díez et al., 2009). Total mercury hair concentration in children correlates with fish consumption frequency and differs between populations from different regions. Thus, this risk characterization could be further enhanced by addressing the limited availability of HBM data, specifically for children below age of five years from different regions.

## 3.6. Study limitations

Several limitations and future implications need to be considered when applying our established PBK model for long-term exposure modeling in dietary risk assessment. Firstly, the established PBK model was only evaluated using body, consumption, and exposure biomarker data from the French population. However, those data vary from one population to another and are highly interlinked. Generally, the French population older than 18 years has slightly higher mercury hair concentrations than the median level of 0.3 µg/g reported for European populations (Basu et al., 2018), most likely due to a higher seafood consumption. Therefore, future studies are needed to evaluate the established PBK model across various populations with different seafood consumptions and mercury concentrations in seafood, specifically for children younger than five years of age.

Secondly, the established PBK model was evaluated using organ concentrations from autopsied individuals, which may influence toxicokinetic processes. Postmortem organ concentrations might have been changed by several factors like redistribution, diffusion, bacterial activity, and biotransformation alterations (Stephenson et al., 2024). For instance, chemical diffusion can be affected due to the absence of oxygen and the loss of maintaining energy-dependent concentration gradients due to the cessation of ATP production. Anaerobic metabolism, loss of membrane integrity associated with autolysis, and pH decrease are also factors that might have influenced postmortem organ concentrations.

Even though there is a clear need to understand better the effect of the complex postmortem processes on organ concentration changes, our established mercury PBK model estimated mercury concentrations in hair sampled from the Esteban participants well, but less so the total mercury concentrations in urine.

Thirdly, the toxicokinetic processes might differ between lower real lifetime intakes and higher regulatory-relevant intakes like maximum levels in seafood and HBGV. However, those dose-dependent processes have not been considered in the simulations, which could be a potential source of bias in estimating mercury hair and urine concentrations based on high-intake seafood consumption scenarios in our risk assessment approach. Toxicokinetic processes might also change with age, which needs to be considered when applying different toxicokinetic parameter values.

A fourth limitation is that pre- and postnatal exposure was not considered as an event in this lifetime PBK model, despite being an important exposure window (Crépet et al., 2022; Ou et al., 2018). Including foetal exposure during pregnancy and breastfeeding as an additional exposure source might alter the estimated dynamics of mercury concentrations in hair. In the case of prenatal mercury exposure, average hair concentrations of 1.68 μg/g in Spanish newborns were higher than in preschool children with 0.94 μg/g of total mercury in hair (Díez et al., 2008). Physiological equations for pregnancy were reviewed in a previous study, which may be added to this library to estimate the internal dose from conception (Thépaut et al., 2023).

This study has also not considered the evolution of important enzyme and transporter kinetics. Therefore, we suggest implementing a coherent evolution of enzymes and transporters in lifetime PBK models that reflect the dynamics of enzyme abundances and metabolization capabilities across life stages (El-Masri et al., 2016). Even though the evolution of chemical-specific enzymes and transporters over life has been previously considered (Beaudouin et al., 2010), the challenge relies on creating equations for the different enzymes and transporters potentially useable for any chemical (Gonnabathula et al., 2024).

Lastly, our refined risk assessment approach indicated that the current consumption of food at any time point in life is suggested to be regarded without health concerns for neurodevelopmental effects and renal effects in the regarded French population, even at the upper uncertainty intervals that stochastically accounted for population variability of dietary intakes and body parameters. However, this assessment needs to be validated for other populations with a broad range of dietary exposure scenarios, including high seafood consumers and additional iHg exposure sources than just food. A Bayesian framework (e.g., MCMC) could be of interest in future work to consider uncertainties and variability across different populations, including estimations of daily intakes. It has to be also noted that this risk characterization did not consider potential additive/independent mixture effects. In addition, our health is positively affected by food highly packed with nutrients and minerals, such as consuming seafood as a resource for essential omega-3 fatty acids, vitamin A, and vitamin B. Therefore, a balance between food consumption's benefits and risks for various potential effects needs to be considered as well.

### *3.7. Established tools for future lifetime risk assessment applications*

Two tools were produced for future PBK model applications based on the inventory of physiological equations. An Excel spreadsheet was created to facilitate a user-friendly and efficient application (Supplement). The user can choose to calculate organ volumes for both sexes based on either default age-dependent body weight and height or specific body parameters. Individual calculations were provided based on each physiological equation and statistics on age-specific organ volumes and fractions of organ volumes. The statistical summary included mean, standard deviation, and coefficient of variances and can be implemented in future age-specific PBK models for a more harmonized application of the Next Generation PBK models.

A code was created in R illustrating the applicability of lifetime physiological equations for an age-specific PBK model. To this end, an age-specific PBK model was modified to model chronic exposure from dietary total mercury intake as a case study. We applied several sets of physiology equations extracted from various lifetime PBK models and compared the simulated output with HBM data. We provide R files used to simulate organ volume growths based on the physiological equations extracted from the different lifetime PBK models. Organ volume growths in the PBK model for total mercury can be simulated using a variety of inventoried physiological equations.

## 4. Conclusion

Our study proposes applicable tools that improve lifetime exposure estimates using PBK models. We have built a library of physiological equations describing organ volume growth that can be added to lifetime PBK models. Using our Excel calculator and R tool (Supplement, GitHub, Zenodo), these equations can now be easily applied in Next Generation PBK models. Then, we successfully demonstrated how to implement and evaluate long-term exposure in an age-specific PBK model using total mercury (as mixture of iHg and MeHg) as a case study. This novel approach improved internal exposure estimates over a lifetime, considering real-life total mercury exposure from modeled dietary intake and population variabilities. We further demonstrated how to use the established lifetime PBK model for a refined risk assessment of dietary exposure to total mercury. Specifically, we assessed (i) the correlation of measured and estimated mercury concentrations in several biological matrices across life stages and (ii) the estimation of mercury concentrations in hair and urine from lifelong consumption of maximum limits defined by regulation in seafood items and HBGV intakes. To conclude, this study demonstrates the applicability of a lifetime PBK model in the risk assessment of a chemical mixture that accounted for exposure dynamics due to body growth and changes in food consumption from imputed MeHg and iHg intakes over life.

## CRediT authorship contribution statement

**Thomas Gastellu:** Writing – review & editing, Writing – original draft, Visualization, Validation, Software, Investigation, Formal analysis, Data curation, Conceptualization. **Achilleas Karakoltzidis:** Writing – review & editing, Writing – original draft, Funding acquisition, Conceptualization. **Aude Ratier:** Writing – review & editing, Writing – original draft, Software, Funding acquisition, Formal analysis, Conceptualization. **Marie Bellouard:** Writing – review & editing, Data curation. **Jean-Claude Alvarez:** Writing – review & editing, Data curation. **Bruno Le Bizec:** Writing – review & editing, Supervision, Funding acquisition. **Gilles Rivière:** Writing – review & editing, Supervision, Funding acquisition. **Spyros Karakitsios:** Writing – review & editing, Supervision, Funding acquisition. **Dimosthenis A. Sarigiannis:** Writing – review & editing, Supervision, Funding acquisition. **Carolina Vogs:** Writing – review & editing, Writing – original draft, Supervision, Software, Funding acquisition, Formal analysis, Conceptualization.

## Declaration of competing interest

The authors declare that they have no known competing financial interests or personal relationships that could have appeared to influence the work reported in this paper.

## Acknowledgment

This project has received funding from the European Partnership for the Assessment of Risks from Chemicals (PARC project) founded by the European Union's Horizon Europe research and innovation programme under Grant Agreement No 101057014, and from FORMAS a Swedish council for sustainable development [Grant No 2023-00591]. This study

was supported by ANSES and INRAE (thesis scholarship co-financing agreement).

## Appendix A. Supplementary data

Supplementary data to this article can be found online at https://doi.org/10.1016/j.envres.2024.120393.

## Data availability

The authors do not have permission to share data.

## References


Abass, K., Huusko, A., Knutsen, H.K., Nieminen, P., Myllynen, P., Meltzer, H.M., Vahakangas, K., Rautio, A., 2018. Quantitative estimation of mercury intake by toxicokinetic modelling based on total mercury levels in humans. Environ. Int. 114, 1–11. https://doi.org/10.1016/j.envint.2018.02.028.

Altman, P. L., and Dittmer, D. S., 1962. Biological Handbook : Growth, Including Reproduction and Morphological Development. Federation of American Societies for Experimental Biology, Washington, D.C., 608 pp. Science, 140(3567), 638-639. https://doi.org/10.1126/science.140.3567.638.c.

AFSSA, 2006. Etude des consommations alimentaires de produits de la mer et impregnation aux elements traces, polluants et omega 3(CALIPSO) [Study of consumption of seafood and body burden to trace elements. pollutants and omega 3 (CALIPSO)]. https://www.anses.fr/en/system/files/PASER-Ra-CalipsoEN.pdf.

ANSES, 2011. Étude de l'alimentation totale française 2 (EAT 2) Tome 2. https://www.anses.fr/fr/system/files/PASER2006sa0361.pdf.

ANSES, 2016. Etude de l'alimentation totale infantile: avis de l'Anses, synthese et conclusions [Infant Total Diet Study: anses' opinion, synthesis and conclusions]. Maisons-Alfort: ANSES. https://www.anses.fr/fr/system/files/ERCA2010SA0317Ra.pdf.

ANSES, 2017. Étude Individuelle Nationale Des Consommations Alimentaires 3 (INCA 3). Maisons-Alfort. https://www.anses.fr/sites/default/files/NUT2014SA0234Ra.pdf.

Arnold, S.M., Angerer, J., Boogaard, P.J., Hughes, M.F., O'Lone, R.B., Robison, S.H., Robert Schnatter, A., 2013. The use of biomonitoring data in exposure and human health risk assessment: benzene case study. Crit. Rev. Toxicol. 43 (2), 119–153. https://doi.org/10.3109/10408444.2012.756455.

ATSDR, 2022. Toxicological profile for mercury. https://www.atsdr.cdc.gov/toxprofiles/tp46.pdf.

Baron, K.T., Gillespie, B., Margossian, C., 2022. mrgsolve: simulate from ODE-based models. R package version 1 (6). https://cran.r-project.org/web/packages/mrgsolve/mrgsolve.pdf.

Basu, N., Horvat, M., Evers, D.C., Zastenskaya, I., Weihe, P., Tempowski, J., 2018. A state-of-the-science review of mercury biomarkers in human populations worldwide between 2000 and 2018. Environmental Health Perspectives 126 (10), 106001. https://doi.org/10.1289/ehp3904.

Beaudouin, R., Micallef, S., Brochot, C., 2010. A stochastic whole-body physiologically based pharmacokinetic model to assess the impact of inter-individual variability on tissue dosimetry over the human lifespan. Regul. Toxicol. Pharmacol. 57 (1), 103–116. https://doi.org/10.1016/j.yrtph.2010.01.005.

Bellouard, M., de la GrandMaison, G.L., Cappy, J., Grimaldi, L., Lontsi-Djeagou, A., Alvarez, J.-C., 2022. Trace elements repartition in body fluids, hair and organs in an autopsied population evaluated by ICP-MS high resolution. Environ. Toxicol. Pharmacol. 95, 103978. https://doi.org/10.1016/j.etap.2022.103978.

Beronius, A., Zilliacus, J., Hanberg, A., Luijten, M., van der Voet, H., van Klaveren, J., 2020. Methodology for health risk assessment of combined exposures to multiple chemicals. Food Chem. Toxicol. 143, 111520. https://doi.org/10.1016/j.fct.2020.111520.

Bizjak, T., Capodiferro, M., Deepika, D., Dinçkol, Ö., Dzhedzheia, V., Lopez-Suarez, L., Petridis, I., Runkel, A.A., Schultz, D.R., Kontić, B., 2022. Human biomonitoring data in health risk assessments published in peer-reviewed journals between 2016 and 2021: confronting reality after a preliminary review. Int. J. Environ. Res. Publ. Health 19 (6), 3362. https://doi.org/10.3390/ijerph19063362.

Brown, R.P., Delp, M.D., Lindstedt, S.L., Rhomberg, L.R., Beliles, R.P., 1997. Physiological parameter values for physiologically based pharmacokinetic models. Toxicol. Ind. Health 13 (4), 407–484. https://doi.org/10.1177/074823379701300401.

Buist, H., 2010. Characterization and application of physiologically based pharmacokinetic models in risk assessment. https://iris.who.int/bitstream/handle/10665/44495/9789241500906_eng.pdf?sequence=1&isAllowed=y.

Carrier, G., Bouchard, M., Brunet, R.C., Caza, M., 2001. A toxicokinetic model for predicting the tissue distribution and elimination of organic and inorganic mercury following exposure to methyl mercury in animals and humans. II. Application and validation of the model in humans. Toxicol. Appl. Pharmacol. 171 (1), 50–60. https://doi.org/10.1006/taap.2000.9113.

Crépet, A., Vasseur, P., Jean, J., Badot, P.-M., Nesslany, F., Vernoux, J.-P., Feidt, C., Mhaouty-Kodja, S., 2022. Integrating selection and risk assessment of chemical mixtures: a novel approach applied to a breast milk survey. Environmental Health Perspectives 130 (3), 035001. https://doi.org/10.1289/ehp8262.

Dede, E., Tindall, M.J., Cherrie, J.W., Hankin, S., Collins, C., 2018. Physiologically-based pharmacokinetic and toxicokinetic models for estimating human exposure to five toxic elements through oral ingestion. Environ. Toxicol. Pharmacol. 57, 104–114. https://doi.org/10.1016/j.etap.2017.12.003.

Deepika, D., Kumar, V., 2023. The role of "physiologically based pharmacokinetic model (PBPK)" new approach methodology (NAM) in pharmaceuticals and environmental chemical risk assessment. Int. J. Environ. Res. Publ. Health 20 (4), 3473. https://doi.org/10.3390/ijerph20043473.

Deepika, D., Sharma, R.P., Schuhmacher, M., Kumar, V., 2021. Risk assessment of perfluorooctane sulfonate (PFOS) using dynamic age dependent physiologically based pharmacokinetic model (PBPK) across human lifetime. Environ. Res. 199, 111287.

Díez, S., Delgado, S., Aguilera, I., et al., 2009. Prenatal and early childhood exposure to mercury and methylmercury in Spain, a high-fish-consumer country. Arch. Environ. Contam. Toxicol. 56, 615–622. https://doi.org/10.1007/s00244-008-9213-7.

Doménech, E., Martorell, S., 2024. Review of the terminology, approaches, and formulations used in the guidelines on quantitative risk assessment of chemical hazards in food. Foods 13 (5), 714. https://doi.org/10.3390/foods13050714.

Dopart, P.J., Friesen, M.C., 2017. New opportunities in exposure assessment of occupational epidemiology: use of measurements to aid exposure reconstruction in population-based studies. Current environmental health reports 4, 355–363. https://doi.org/10.1007/s40572-017-0153-0.

EFSA, 2011. Scientific Opinion on the risks for public health related to the presence of zearalenone in food. EFSA J. 9 (6), 2197. https://doi.org/10.2903/j.efsa.2011.2197.

EFSA, 2012. Scientific Opinion on the risk for public health related to the presence of mercury and methylmercury in food. EFSA J. 10 (12), 2985. https://doi.org/10.2903/j.efsa.2012.2985.

EFSA, 2021. Technical report on handling occurrence data for dietary exposure assessments. EFSA Supporting Publications 18. https://doi.org/10.2903/sp.efsa.2021.en-7082.

El-Masri, H., Kleinstreuer, N., Hines, R.N., Adams, L., Tal, T., Isaacs, K., Wetmore, B.A., Tan, Y.-M., 2016. Integration of life-stage physiologically based pharmacokinetic models with adverse outcome pathways and environmental exposure models to screen for environmental hazards. Toxicol. Sci. 152 (1), 230–243. https://doi.org/10.1093/toxsci/kfw082.

Esteban-López, M., Arrebola, J.P., Juliá, M., Pärt, P., Soto, E., Cañas, A., Pedraza-Díaz, S., González-Rubio, J., Castaño, A., 2022. Selecting the best non-invasive matrix to measure mercury exposure in human biomonitoring surveys. Environ. Res. 204, 112394. https://doi.org/10.1016/j.envres.2021.112394.

European Commission, 2023. Commission Regulation (EU) 2023/915 on maximum levels for certain contaminants in food and repealing Regulation (EC) No 1881/2006.

Gastellu, T., Mondou, A., Bellouard, M., Alvarez, J.-C., Le Bizec, B., Rivière, G., 2024. Characterizing the risk related to the exposure to methylmercury over a lifetime: a global approach using population internal exposure. Food Chem. Toxicol. 114598. https://doi.org/10.1016/j.fct.2024.114598.

Gbadamosi, M.R., Abdallah, M.A.-E., Harrad, S., 2021. A critical review of human exposure to organophosphate esters with a focus on dietary intake. Sci. Total Environ. 771, 144752. https://doi.org/10.1016/j.scitotenv.2020.144752.

Georgopoulos, P.G., Sasso, A.F., Isukapalli, S.S., Lioy, P.J., Vallero, D.A., Okino, M., Reiter, L., 2009. Reconstructing population exposures to environmental chemicals from biomarkers: challenges and opportunities. J. Expo. Sci. Environ. Epidemiol. 19 (2), 149–171. https://doi.org/10.1038/jes.2008.9.

Gonnabathula, P., Choi, M.-K., Li, M., Kabadi, S.V., Fairman, K., 2024. Utility of life stage-specific chemical risk assessments based on New Approach Methodologies (NAMs). Food Chem. Toxicol. 190, 114789. https://doi.org/10.1016/j.fct.2024.114789.

Goullé, J.-P., Mahieu, L., Anagnostides, J.-G., Bouige, D., Saussereau, E., Guerbet, M., Lacroix, C., 2010. Profil métallique tissulaire par ICP-MS chez des sujets décédés. Annales de Toxicologie Analytique.

Grandjean, P., Weihe, P., White, R.F., et al., 1997. Cognitive deficit in 7-year-old children with prenatal exposure to methylmercury. Neurotoxicol. Teratol. 19, 417–428.

Haddad, S., Restieri, C., Krishnan, K., 2001. Characterization of age-related changes in body weight and organ weights from birth to adolescence in humans. J. Toxicol. Environ. Health, Part A 64 (6), 453–464. https://doi.org/10.1080/152873901753215911.

Haddad, S., Tardif, G.-C., Tardif, R., 2006. Development of physiologically based toxicokinetic models for improving the human indoor exposure assessment to water contaminants: trichloroethylene and trihalomethanes. J. Toxicol. Environ. Health, Part A 69 (23), 2095–2136. https://doi.org/10.1080/15287390600631789.

Harttig, U, Haubrock, J, Knüppel, S, Boeing, H, 2011. EFCOVAL Consortium. The MSM program: web-based statistics package for estimating usual dietary intake using the Multiple Source Method. Eur J Clin Nutr. https://doi.org/10.1038/ejcn.2011.92.

HBM4EU, 2018. Biomarkers of effect: what you need to know. Retrieved from. https://www.hbm4eu.eu/wp-content/uploads/2018/12/Biomarkers-of-effects-factsheet_EN_final-1.pdf.

ICRP, 2002. Basic anatomical and physiological data for use in radiological protection reference values. ICRP Publication 89. Ann. ICRP 32 (3–4).

Jeddi, M.Z., Hopf, N.B., Louro, H., Viegas, S., Galea, K.S., Pasanen-Kase, R., Santonen, T., Mustieles, V., Fernandez, M.F., Verhagen, H., 2022. Developing human biomonitoring as a 21st century toolbox within the European exposure science strategy 2020–2030. Environ. Int. 168, 107476. https://doi.org/10.1016/j.envint.2022.107476.

Kim, K.-H., Kabir, E., Jahan, S.A., 2016. A review on the distribution of Hg in the environment and its human health impacts. J. Hazard Mater. 306, 376–385. https://doi.org/10.1016/j.jhazmat.2015.11.031.

Mallick, P., Moreau, M., Song, G., Efremenko, A.Y., Pendse, S.N., Creek, M.R., Osimitz, T. G., Hines, R.N., Hinderliter, P., Clewell, H.J., 2020. Development and application of

a life-stage physiologically based pharmacokinetic (PBPK) model to the assessment of internal dose of pyrethroids in humans. Toxicol. Sci. 173 (1), 86–99. https://doi.org/10.1093/toxsci/kfz211.

McCarty, L., Landrum, P., Luoma, S., Meador, J., Merten, A., Shephard, B., Van Wezel, A., 2011. Advancing environmental toxicology through chemical dosimetry: external exposures versus tissue residues. Integrated Environ. Assess. Manag. 7 (1), 7–27. https://doi.org/10.1002/ieam.98.

McDowell, M.A., Dillon, C.F., Osterloh, J., et al., 2004. Hair mercury levels in US children and women of childbearing age: reference range data from NHANES 1999–2000. Environment Health Perspective 112, 1165–1171.

McNally, K., Cotton, R., Hogg, A., Loizou, G., 2014. PopGen: a virtual human population generator. Toxicology 315, 70–85. https://doi.org/10.1016/j.tox.2013.07.009.

Nuttall, K.L., 2004. Interpreting mercury in blood and urine of individual patients. Ann. Clin. Lab. Sci. 34 (3), 235–250. http://www.annclinlabsci.org/content/34/3/235.full.pdf+html.

Oleko, A., Saoudi, A., Zeghnoun, A., Pecheux, M., Cirimele, V., Mihai Cirtiu, C., Berail, G., Szego, E., Denys, S., Fillol, C., 2024. Exposure of the general French population to metals and metalloids in 2014-2016: results from the Esteban study. Environ. Res. 252 (Pt 2), 118744.

Ou, L., Wang, H., Chen, C., Chen, L., Zhang, W., Wang, X., 2018. Physiologically based pharmacokinetic (PBPK) modeling of human lactational transfer of methylmercury in China. Environ. Int. 115, 180–187. https://doi.org/10.1016/j.envint.2018.03.018.

Pendse, S.N., Efremenko, A., Hack, C.E., Moreau, M., Mallick, P., Dzierlenga, M., Nicolas, C.I., Yoon, M., Clewell, H.J., McMullen, P.D., 2020. Population Life-course exposure to health effects model (PLETHEM): an R package for PBPK modeling. Computational Toxicology 13, 100115. https://doi.org/10.1016/j.comtox.2019.100115.

Pope, Q., Rand, M.D., 2021. Variation in methylmercury metabolism and elimination in humans: physiological pharmacokinetic modeling highlights the role of gut biotransformation, skeletal muscle, and hair. Toxicol. Sci. 180 (1), 26–37. https://doi.org/10.1093/toxsci/kfaa192.

Price, K., Haddad, S., Krishnan, K., 2003. Physiological modeling of age-specific changes in the pharmacokinetics of organic chemicals in children. J. Toxicol. Environ. Health, Part A 66 (5), 417–433. https://doi.org/10.1080/15287390306450.

Pruvost-Couvreur, M., Le Bizec, B., Béchaux, C., Rivière, G., 2020a. Dietary risk assessment methodology: how to deal with changes through life. Food Addit. Contam. 37 (5), 705–722. https://doi.org/10.1080/19440049.2020.1727964.

Pruvost-Couvreur, M., Le Bizec, B., Béchaux, C., Rivière, G., 2020b. A method to assess lifetime dietary risk: example of cadmium exposure. Food Chem. Toxicol. 137, 111130. https://doi.org/10.1016/j.fct.2020.111130.

Pruvost-Couvreur, M., Béchaux, C., Rivière, G., Le Bizec, B., 2021. Impact of sociodemographic profile, generation and bioaccumulation on lifetime dietary and internal exposures to PCBs. Sci. Total Environ. 800, 149511. https://doi.org/10.1016/j.scitotenv.2021.149511.

Ratier, A., et al., 2023. Inventory of PBK models for assessing the internal exposure through life. PARC report. https://www.eu-parc.eu/sites/default/files/2023-08/PARC_AD6.4.pdf.

Ring, C.L., Pearce, R.G., Setzer, R.W., Wetmore, B.A., Wambaugh, J.F., 2017. Identifying populations sensitive to environmental chemicals by simulating toxicokinetic variability. Environ. Int. 106, 105–118. https://doi.org/10.1016/j.envint.2017.06.004.

Ruebenacker, O., Moraru, I.I., Schaff, J.C., Blinov, M.L., 2007. Kinetic modeling using BioPAX ontology. 2007 IEEE International Conference on Bioinformatics and Biomedicine.Fremont, CA, USA, pp. 339-348, doi: 10.1109/BIBM.2007.55.

Santonen, T., Mahiout, S., Alvito, P., Apel, P., Bessems, J., Bil, W., Borges, T., Bose-O'Reilly, S., Buekers, J., Portilla, A.I.C., 2023. How to use human biomonitoring in chemical risk assessment: methodological aspects, recommendations, and lessons learned from HBM4EU. Int. J. Hyg Environ. Health 249, 114139. https://doi.org/10.1016/j.ijheh.2023.114139.

Sarigiannis, D.A., Karakitsios, S.P., Handakas, E., Gotti, A., 2020. Development of a generic lifelong physiologically based biokinetic model for exposome studies. Environ. Res. 185, 109307. https://doi.org/10.1016/j.envres.2020.109307.

Schlender, J.-F., Meyer, M., Thelen, K., Krauss, M., Willmann, S., Eissing, T., Jaehde, U., 2016. Development of a whole-body physiologically based pharmacokinetic approach to assess the pharmacokinetics of drugs in elderly individuals. Clin. Pharmacokinet. 55, 1573–1589. https://doi.org/10.1007/s40262-016-0422-3.

Sirot, V., Guérin, T., Mauras, Y., Garraud, H., Volatier, J.-L., Leblanc, J.-C., 2008. Methylmercury exposure assessment using dietary and biomarker data among frequent seafood consumers in France: CALIPSO study. Environ. Res. 107 (1), 30–38. https://doi.org/10.1016/j.envres.2007.12.005.

Smith, J.N., Hinderliter, P.M., Timchalk, C., Bartels, M.J., Poet, T.S., 2014. A human life-stage physiologically based pharmacokinetic and pharmacodynamic model for chlorpyrifos: development and validation. Regul. Toxicol. Pharmacol. 69 (3), 580–597. https://doi.org/10.1016/j.yrtph.2013.10.005.

Stephenson, L., Van Den Heuvel, C., Scott, T., Byard, R.W., 2024. Difficulties associated with the interpretation of postmortem toxicology. J. Anal. Toxicol. 13 (48), 405–412. https://doi.org/10.1093/jat/bkae052.

Thépaut, E., Brochot, C., Chardon, K., Personne, S., Zeman, F., 2023. Pregnancy-PBPK models: how are biochemical and physiological processes integrated? Computational Toxicology, 100282. https://doi.org/10.1016/j.comtox.2023.100282.

Tooze, J.A., Midthune, D., Dodd, K.W., Freedman, L.S., Krebs-Smith, S.M., Subar, A.F., Guenther, P.M., Carroll, R.J., Kipnis, V., 2006. A New Statistical Method for Estimating the Usual Intake of Episodically Consumed Foods with Application to Their Distribution. Journal Of The American Dietetic Association 106, 1575–1587. https://doi.org/10.1016/j.jada.2006.07.003.

Verner, M.-A., Charbonneau, M., López-Carrillo, L., Haddad, S., 2008. Physiologically based pharmacokinetic modeling of persistent organic pollutants for lifetime exposure assessment: a new tool in breast cancer epidemiologic studies. Environmental Health Perspectives 116 (7), 886–892. https://doi.org/10.1289/ehp.10917.

WHO and IPCS, 2010. Characterization and Application of Physiologically Based Phamacokinetic Models in Risk Assessment. World Health Organization, Geneva, Switzerland. https://apps.who.int/iris/handle/10665/44495.

WHO and IPCS, 2021. WHO human health risk assessment toolkit: chemical hazards. Retrieved from. https://iris.who.int/bitstream/handle/10665/350206/9789240035720-eng.pdf?sequence=1&isAllowed=y.

Wu, H., Yoon, M., Verner, M.-A., Xue, J., Luo, M., Andersen, M.E., Longnecker, M.P., Clewell, H.J., 2015. Can the observed association between serum perfluoroalkyl substances and delayed menarche be explained on the basis of puberty-related changes in physiology and pharmacokinetics? Environ. Int. 82, 61–68. https://doi.org/10.1016/j.envint.2015.05.006.

Yoon, H., Kim, T.H., Lee, B.-c., Lee, B., Kim, P., Shin, B.S., Choi, J., 2022. Comparison of the exposure assessment of di (2-ethylhexyl) phthalate between the PBPK model-based reverse dosimetry and scenario-based analysis: A Korean general population study. Chemosphere 294, 133549. https://doi.org/10.1016/j.chemosphere.2022.133549.

Zhang, F., Erskine, T., McClymont, E., Moore, L., LeBaron, M., McNett, D., Marty, S., 2024. Predictions of tissue concentrations of myclobutanil, oxyfluorfen, and pronamide in rat and human after oral exposures via GastroPlusTM physiologically based pharmacokinetic modelling. SAR QSAR Environ. Res. 35 (4), 285–307. https://doi.org/10.1080/1062936x.2024.2333878.